A STUDY OF THE EFFECT OF HOST GALAXY EXTINCTION ON THE COLORS OF TYPE IA SUPERNOVAE

Aleksandar Cikota

Submitted to the
INSTITUTE FOR ASTRO- AND PARTICLE PHYSICS
of the
UNIVERSITY OF INNSBRUCK
AstroMundus Programme

in Partial Fulfillment of the Requirements for the Degree of
MAGISTER DER NATURWISSENSCHAFTEN
(Master of Science, MSc)

in Astronomy & Astrophysics

Supervised by:
Assoc. Prof. Francine Marleau, Univ. Prof. Dr. Norbert Przybilla

Innsbruck, July 2015

Preface

The reserch for this Master's thesis was partially conducted at the Space Telescope Science Institute in Balimore, MD, USA, during a 15 weeks internship hosted by Dr. Susana Deustua. Also, a manuscript containing the research conducted for this master thesis, entitled "Determining Type Ia Supernovae host galaxy extinction probabilities and a statistical approach to estimating the absorption-to-reddening ratio R_V" by Aleksandar Cikota, Susana Deustua, and Francine Marleau, was submitted to *The Astrophysical Journal* on May 13th, 2015.

Aleksandar Cikota
Baltimore, June 2015

Abstract

We aim to place limits on the extinction values of Type Ia supernovae to statistically determine the most probable color excess, E(B-V), with galactocentric distance, and to use these statistics to determine the absorption-to-reddening ratio, R_V, for dust in the host galaxies.

We determined pixel-based dust mass surface density maps for 59 galaxies from the Key Insight on Nearby Galaxies: a Far-Infrared Survey with *Herschel* (KINGFISH, Kennicutt et al. (2011)). We use Type Ia supernova spectral templates (Hsiao et al., 2007) to develop a Monte Carlo simulation of color excess E(B-V) with R_V=3.1 and investigate the color excess probabilities E(B-V) with projected radial galaxy center distance. Additionally, we tested our model using spectra of SN 1989B, SN 2002bo and SN 2006X, which occurred in three KINGFISH galaxies.

Finally, we determined the most probable reddening for Sa-Sap, Sab-Sbp, Sbc-Scp, Scd-Sdm, S0 and Irregular galaxy classes as a function of R/R_{25}, and found that the largest reddening probability are expected in Sab-Sb and Sbc-Sc galaxies, while S0 and Irregulars are very dust poor. We present a new approach for determining the absorption-to-reddening ratio R_V using color excess probability functions, and find for a sample of 21 SNe Ia observed in Sab-Sbp galaxies, and 34 SNe in Sbc-Scp, an R_V of 2.71 $\pm$ 1.58 and R_V = 1.70 $\pm$ 0.38 respectively.

Contents

Chapter 1

Introduction

1.1 Motivation and goals

Because Type Ia supernovae (SNe Ia) are bright, they are good standard candles and probably the most accurate distance indicators on cosmological scales. Although SNe Ia are not equally bright there is a known correlation between their peak brightness and the width of their light curves (Phillips, 1993), which is used to standardize the "Branch" normal SNe Ia. However, there are SNe Ia that appear dimmer and redder than the Branch normals, either because they are intrinsically different, or because they suffer greater host galaxy extinction. One of the largest sources of uncertainty in Type Ia SNe photometric measurements is the extinction due to the host galaxy, which affects the accuracy and precision of constructed Hubble diagrams. In turn, this limits the accuracy of the measurement of the dark energy parameters. Sullivan et al. (2006) examined the effect of host galaxy morphology on the Hubble diagram of SNe Ia. They found that elliptical galaxy SNe Hubble diagram had less scatter than spiral galaxy SNe.

Understanding the effect of dust extinction on SNe Ia is essential for accurate measurement of cosmological parameters and the expansion history of the Universe (Riess et al., 1998; Perlmutter et al., 1999). Extinction A_V, is determined from the reddening law $E(B-V) = A_V/R_V$, where the color excess E(B-V) depends on the properties of dust. If these are uncertain and/or evolve with redshift, the extinction, and thus the SNe Ia brightness, might be systematically wrong.

Previous studies of the extinction from SNe Ia (summarized in Table 1.1) yielded diverse values of the absorption to reddening ratio, R_V, ranging from R_V = 1 to R_V = 3.0. For comparison, the average value for the Milky Way is R_V = 3.1. These studies used a variety of methods to calculate R_V, most of them are variants on light curve fitting.

Branch and Tammann (1992) calculated R_B = 2.0 from measurements of six SNe Ia in the Virgo cluster, and R_B = 1.2 from three pairs of SNe which occurred in the same galaxies (note that R_B = R_V + 1). They also determined R_B = 1.3 $\pm$ 0.2 from a least square solution for a sample of 17 nearby SNe Ia ($\lesssim$ 4000 $km\ s^{-1}$) in the Hubble diagram, using the SNe Ia sample from Miller and Branch (1990). In contrast, Phillips et al. (1999) developed a method to estimate the extinction of low redshift SNe Ia (0.01 $\lesssim$ z $\lesssim$ 0.1) based on the observational coincidence that the B-V evolution between 30 and 90 days after the peak luminosity in V is similar for all SNe Ia, regardless of lightcurve shape. They obtain R_V = 3.5 $\pm$ 0.4 for a sample of 49 SNe Ia.

Altavilla et al. (2004) estimated R_B = 3.5 from light curves of 73 SNe with z $\lesssim$ 0.1. Reindl et al. (2005) calculated R_V = 2.65 $\pm$ 0.15 for 111 SNe Ia with recession velocities between 3000 $km\ s^{-1}$ and 20000 $km\ s^{-1}$, exploiting the M_B(max) vs. E(B-V) correlation. Riess et al. (1996) found a value of R_V = 2.55 $\pm$ 0.30, derived using a multicolor

light-curve shape (MLCS) method for a sample of 20 Ia SNe with z $\lesssim$ 0.1. Conley et al. (2007) used four different light curve fitting packages, and determined $R_V \sim 1$ for a sample of 61 SNe with v $\lesssim$ 40000 $km\ s^{-1}$. To explain their low R_V, Conley et al. (2007) suggest that a more complicated model of intrinsic SN colors is required, which goes beyond single light-curve shape-color relation, or that dust in the host galaxies of the Ia SNe is quite atypical compared to Milky Way dust.

In a different approach, Mandel et al. (2011) constructed a statistical model for Type Ia SNe light curves from the visible through the infrared, and applied it to data of 127 SNe from three surveys (PARTIEL, CfA3, Carnegie Supernova Project) and from the literature. They calculated $R_V \approx$ 2.5-2.9 for $A_V \lesssim$ 0.4, while at high extinctions, $A_V \gtrsim 1$, values of $R_V < 2$ are favored. Kessler et al. (2009) determined R_V = 2.18 $\pm$ 0.14(stat) $\pm$ 0.48(syst) by matching observed and predicted SN Ia colors for 103 SNe with 0.04 $<$ z $<$ 0.42. Folatelli et al. (2010) found $R_V \approx 1.7$ when using 17 low-redshift (z $<$ 0.08) SNe Ia monitored by the Carnegie Supernova Project, but obtain $R_V \approx 3.2$ when two highly reddened SNe are excluded.

Lampeitl et al. (2010) from a sample of 361 SDSS-II SNe, z $<$ 0.21, utilizing two light curve methods, found that SNe Ia in passive host galaxies favor a dust law of R_V = 1.0 $\pm$ 0.2, while SNe Ia in star-forming hosts require $R_V = 1.8^{+0.2}_{-0.4}$.

Nobili and Goobar (2008) found that SNe Ia color depends on the light curve shape, such that SNe Ia with fainter, narrower light curves are redder than those with brighter, broader light curves. They correct SNe lightcurves for this intrinsic color difference, and then derive host galaxy reddening. They obtain R_V = 1.75 $\pm$ 0.27 for 80 low redshift ($\lesssim$ 0.1) SNe Ia with $E(B-V) \leq 0.7$ mag, but find that a subset of 69 SNe that have modest reddening, $E(B-V) < 0.25$ mag, have significantly smaller $R_V \sim 1$.

Using a Monte Carlo simulation of circumstellar dust around the supernova location, Goobar (2008) determined $R_V \sim 1.5 - 2.5$ for SNe Ia. One of Goobar's motivations in undertaking this study was the observed steeper dependence with wavelength of the total to selective extinction seen in SNe (by e.g. Wang (2005)). Using Draine's Milky Way dust models (Draine, 2003b) and the Weingartner and Draine (2001) Large Magellanic Clouds dust properties in his simulation, Goobar finds that a simple power law fits the resulting extinction.

Given the apparent inconsistent results in estimating host galaxy extinction from SNe observations, we decided to investigate this problem using a different approach. Our investigation instead uses data obtained in a systematic and consistent way for nearby galaxies to measure the mass and distribution of interstellar medium components (dust), and thence estimate the extinction. The principal goal is to place limits on the uncertainties of SNe Ia extinction values, to estimate the range of host galaxy extinction, i.e. the most probable color excess, in a galaxy sample, and then apply these statistics to a sample of observed Ia SNe in order to infer R_V.

We opted to use the KINGFISH galaxy sample (Key Insight on Nearby Galaxies: a Far-Infrared Survey with *Herschel*, Kennicutt et al., 2011), which when combined with SINGS (Spitzer Infrared Nearby Galaxies Survey (SINGS, Kennicutt et al., 2003), is one of the most complete multi-band surveys of nearby galaxies. Further, Draine et al. (2007), Gordon (2008) and Skibba et al. (2011) have estimated the dust mass of these galaxies. Therefore, these galaxies are an ideal laboratory to explore the effects of dust extinction on SNe Ia.

We first determine the dust density on a per pixel base, then we look at the change in SNe Ia colors with galactocentric distance due to dust extinction.
For galaxies with known SNe Ia, we compare the extincted spectrum template at the po-

Table 1.1: R_V results of earlier studies

REFERENCE	NO. OF SNE	VELOCITY OR REDSHIFT	ABSORPTION-TO-REDDENING RATIO
Branch and Tammann (1992)	6	Nearby (Virgo cluster)	R_B = 2.0
	3 pairs	Nearby	R_B = 1.2
	17	$v \lesssim$ 4000 km s^{-1}	R_B = 1.3 $\pm$ 0.2
Riess et al. (1996)	20	z $\lesssim$ 0.1	R_V = 2.55 $\pm$ 0.30
Phillips et al. (1999)	49	0.01 $\lesssim$ z $\lesssim$ 0.1	R_V = 3.5 $\pm$ 0.4
Altavilla et al. (2004)	73	z $\lesssim$0.1	R_B = 3.5
Reindl et al. (2005)	111	3000 km s^{-1} $< v_{CMB} <$ 20000 km s^{-1}	R_V = 2.65 $\pm$ 0.15
Conley et al. (2007)	28-61	z $\lesssim$ 0.13	$R_V \sim 1$
Mandel et al. (2011)	127	z $\lesssim$ 0.05	$R_V \approx$ 2.5-2.9 for $A_V \lesssim$ 0.4 $R_V <$ 2 for $A_V \gtrsim 1$
Nobili and Goobar (2008)	80	z $\lesssim$ 0.1	$R_V = 1.75 \pm 0.27$ for $E(B-V) \leq 0.7$ mag $R_V \sim$ 1 for $E(B-V) < 0.25$ mag
Kessler et al. (2009)	103	0.04 $<$ z $<$ 0.42	R_V = 2.18 $\pm$ 0.14(stat) $\pm$ 0.48(syst)
Folatelli et al. (2010)	17	z $<$ 0.08	$R_V \approx 1.7$ $R_V \approx$ 3.2 when two reddened SNe excluded
Lampeitl et al. (2010)	361	z $<$ 0.21	R_V = 1.0 $\pm$ 0.2 in passive host $R_V = 1.8^{+0.2}_{-0.4}$ in star-forming hosts
Goobar (2008)	MONTE CARLO SIMULATION		$R_V \sim$ 1.5 - 2.5

sition of the historical supernova to the observed spectra. Finally we present color excess E(B-V) probabilities as functions of galactocentric distance for SNe Ia in different morphological host galaxy types, and use those reddening probability functions to estimate the absorption-to-reddening ratio, R_V, of dust in SNe Ia host galaxies.

In §2 we describe the data, the galaxy dust mass surface density maps, the extinction model, and the spectral templates of SNe Ia. In §3 we describe our Monte Carlo simulation on host galaxy extinction and compare the model to individual Ia observations. In §4 we show and discuss the simulation results, apply them for R_V determination of a Ia SNe sample and discuss the uncertainties. In §5 we summarize the results and conclusions.

1.2 Interstellar dust & dust extinction

Dust grains are formed in the atmospheres of evolved stars, novae and supernovae, and play an important role in the interstellar medium. An important observational effect affected by dust is reddening, caused due to dust extinction, i.e. scattering of photons in directions other than initial, and absorption of photons by the material of the grains. Scattering being wavelength dependent, the scattered light forms reflection nebulae is bluer than that of the illuminating star, while the light transmitted by a dust cloud is redder. The energy being absorbed by dust grains heat them and is re-emitted in the mid- and far-infrared. Almost half of all the energy emitted by stars in the Galaxy in the UV, visible and near infrared is absorbed by dust and then re-emitted at much longer wavelengths. The other half is unaffected or scattered by dust (Lequeux, 2003).

Extinction depends upon grain composition, shape and size distribution and also upon wavelength, and is described by the extinction law, e.g. Cardelli, Clayton, Mathis (1989), as shown in Figure 1.1.

Extinction A_λ in a given waveband (for example V band) equals

$$A_V = m_V - m_{V,0} \tag{1.1}$$

where m_V is apparent V-band magnitude, and $m_{V,0}$ the apparent magnitude in the absence of dust.

The "geneal" extinction A_λ can also be written as terms of the brightness in magnitudes of a source, but this requires knowing its distance and luminosity

$$m_V = M_V + 5logD_L - 5 + A_V \tag{1.2}$$

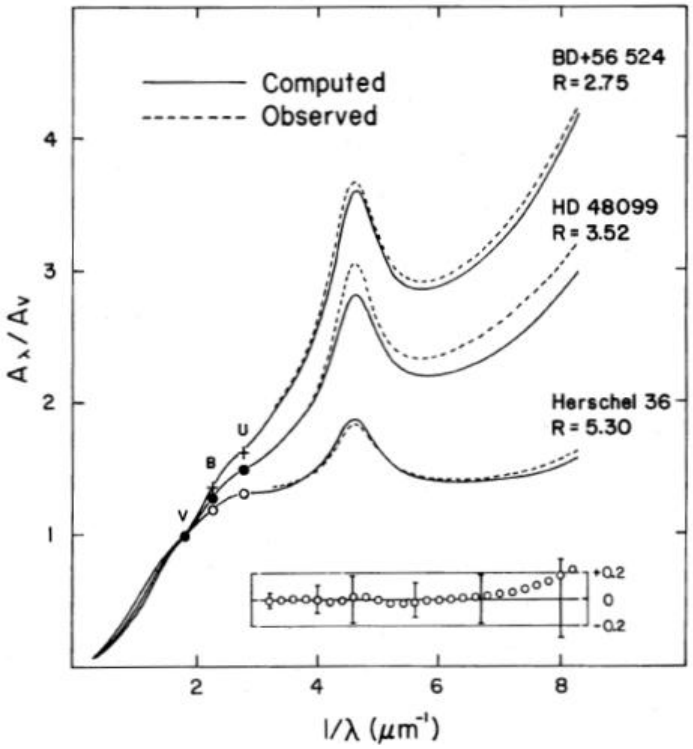

Figure 1.1: Comparison between the mean optical-UV R_V-dependent Cardelli et al. (1989) extinction curves with observations for three different R_V values.

Instead we use the distance-independent "selective extinction" , which is the additional color excess (or reddening) due to extinction:

$$E(B-V) = A_B - A_V = (B-V)_{observed} - (B-V)_{intrinsic} \tag{1.3}$$

where A_B and A_V the extinction in B and V band respectively, (B-V) the reddened color, and $(B-V)_0$ the dereddened color (or unreddened color, or intrinsic color).

The ratio of extinction to reddening (or total to selective absorption):

$$R_V = \frac{A_V}{A_B - A_V} = \frac{A_V}{E(B-V)} \tag{1.4}$$

This ratio is usually known to be approximately constant with the line of sight ($R_V \sim$ 3.1). Adopting this R_V and a known (measured) color excess E(B-V), the extinction can be determined. The reddening E(B-V) can be determined by comparing observed colors with colors derived from the spectral type, from multicolor photometry, or for our Milky way, from reddening maps derived for the entire Galaxy.

1.3 Type Ia supernovae

There are nearly 200 supernovae (SNe) detected each year (IAU Central Bureau for Astronomical Telegrams[1]) which reveals an large number of peculiar supernovae not easy to classify. On the other hand, a large number of supernovae makes detailed studies on a specific class of supernovae possible, and to find correlations between them.

From the observations, it is very clear that there are two main classes of supernovae with phisically completely different backgrounds. The core collapse SNe of massive stars

[1] http://cfa-www.harvard.edu/cfa/lists/Supernovae.html

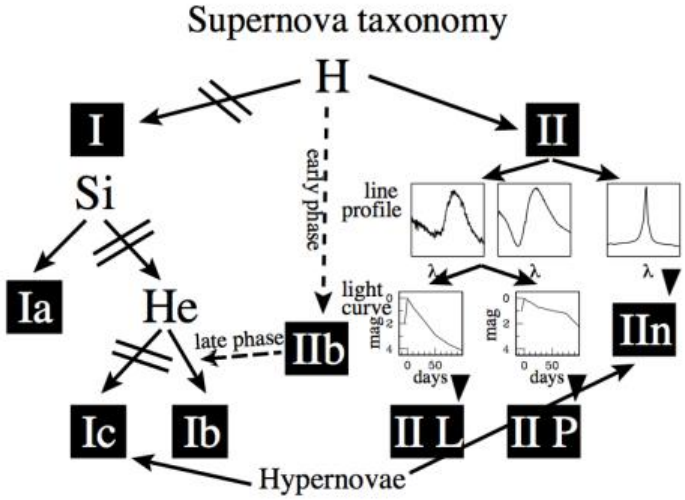

Figure 1.2: Supernova taxonomy. Source: (Cappellaro and Turatto, 2001)

(Type II and Type Ib/c), and Ia SNe. It is universally accepted that type Ia Supernovae are thermonuclear explosion processes of low-mass stars (white dwarfs) in binary systems with red giants. We suppose that the white dwarf explodes after it crosses a critical mass threshold (the Chandrasekhar limit), by accretion of additional material from his binary companion. This threshold should be identical for all Ia SNe, explaining that they all have the same luminosity. Considering their high luminosity, it makes them to ideal standard candles because they can be detected and observed at large distances. However, Ia supernovae are not ideal standard candles, since their peak luminosity varies 0.4 mag in the blue band, but there is a correlation, known as the Phillips relationship, between the peak luminosity and the shape of the light curve, i.e. the speed of luminosity evolution after maximum. The faster the supernova fades from maximum light, the fainter its peak magnitude is. The relation states that the intrinsic peak brightness is given by

$$M_{max}(B) = -21.726 + 2.698\Delta m_{15}(B) \tag{1.5}$$

where $\Delta m_{15}(B)$ is the total amount in magnitudes that the light curve decays from it's peak brightness during 15 days following the peak (Phillips, 1993).

1.3.1 Classification

Supernovae are classified spectroscopicaly according to the absorption lines of different chemical elements that appear in their spectra near the peak luminosity. The fist division is made due to presence or absence of hydrogen lines. Type I SNe contain no hydrogen lines, while Type II show hydrogen lines in their spectra. In each of types divisions there are subdivisions according to the presence of other elements or the shape of light curve. Type I SNe are subdivided to Type Ia which are characterized by the complete absence of helium lines and hydrogen (which never appear in the spectra of Ia SNe at any phase) and a strong absorption line near 6100Å which comes from a doublet of singly ionized silicon with $\lambda\lambda$6347Å and 6371Å. Type I supernovae without this strong Si II line are classified as Type Ib and Ic, with Type Ib showing strong neutral helium lines and Type Ic lacking them. Figure 1.2 shows a detailed clasification of SNe (Cappellaro and Turatto, 2001).

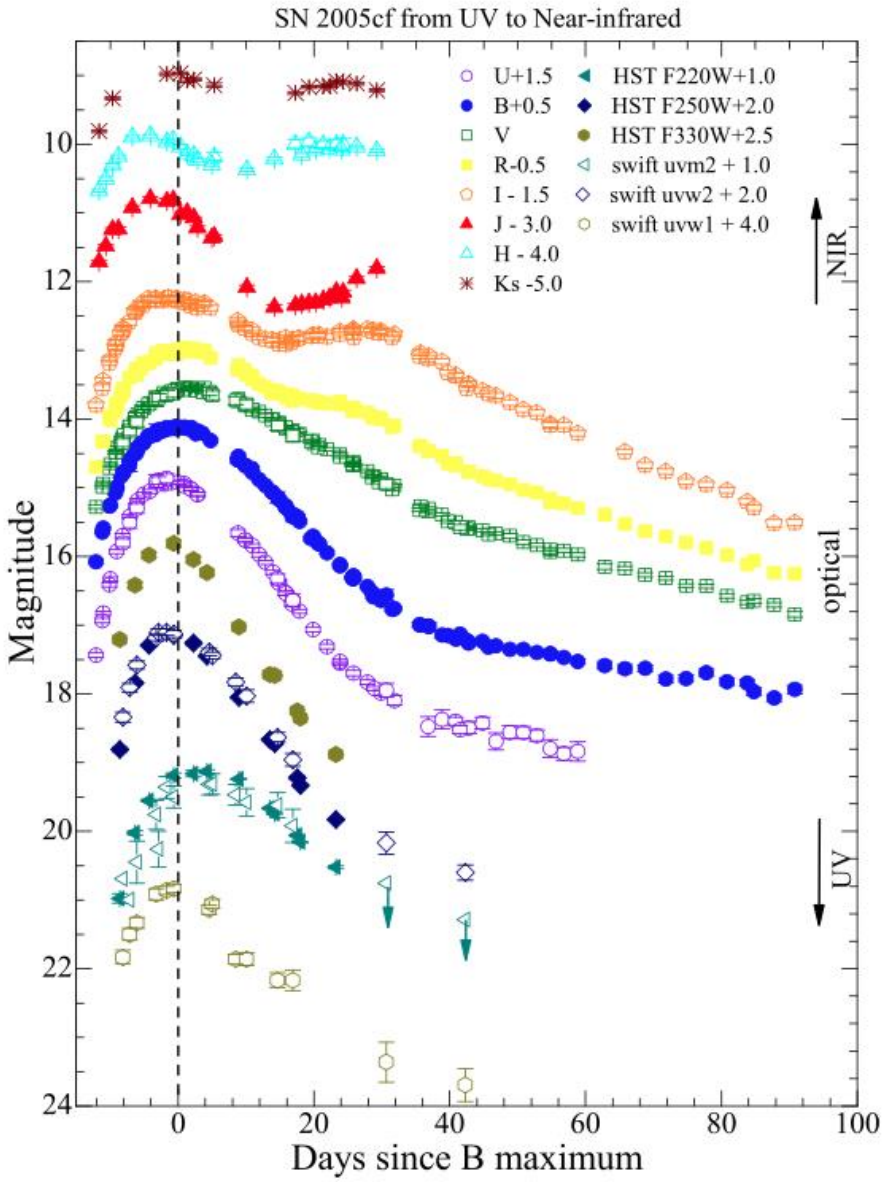

Figure 1.3: The UV, optical, and NIR light curves of SN 2005cf. The UV light curves were obtained from the photometry with HST ACS and the Swift UVOT; the U BV RI optical photometry was collected at eight ground-based telescopes as well as the Swift UVOT; and the JHKs data were taken with the 1.3 m PAIRITEL and with HST NICMOS3 (Wang et al., 2009).

1.3.2 Light curve

Photometric observations of Ia SNe are most common, and therefore light curves are the main source of informaiton about Ia SNe. A typical light curves of Type Ia SN 2005cf in different passbands is shown in Figure 1.3 (Wang et al., 2009). It is common to use the B maximum as the zero-point for the light curves.

The rise times of SNe Ia to maximum is very steep and fast, with about a half magntude per day until about 10 days before maximum. Riess et al. (1999) found that the rise time to B maximum for an SN Ia with Δm_{15}(B) = 1.1 mag and peak M_V = 19.45 mag to be 19.5 $\pm$ 0.2 days. Assuming an expanding fireball with a very slowly changing temperature, the pre maximum light curve can be approximated as t^2 (Riess et al., 1999; Leibundgut, 2000).

The maximum phase starts about 5 days before the peak luminosity in B filter. A typical Ia SNe has already reached its maximum in the near-IR filters JHK (see Figure 1.3) at this time. Around the maximum, the colors envolve rapidly and non-monothonically, compared to the pre-maximum phase when they appear constant. They change from blue (B-V $\approx$ -0.1) at 10 days before to red (B-V $\approx$ 1.1) at 30 days after the maximum.

At maximum, the typical B-V color is about -0.07 $\pm$ 0.03. For the use of Ia SNe as distance in indicators and the measurement of the Hubble constant, it's essential to know the luminosity at peak brightness. The most precise values are derived from nearby supernovae. Saha et al. (1999) determined the distance to SN 1989B using Cepheids, combined his measurement with 8 other calibrations, and calculated the mean absolute magnitudes at maximum of $< M_B >$= -19.48 $\pm$ 0.07 and $< M_V >$ = -19.48 $\pm$ 0.07 for "Branch normal" Ia SNe.

A second maximum has been observed between days 21 and 30 after the B maximum in the I and redder light curves. However, it's interpretation is still not completely clear. After about 50 days, the decline rates become steady and are basically the same for all Ia SNe. The B light curve decline rate is about 0.014mag/day, and the V about 0.028 mag/day. After around 150 days, the SNe is about 5 mag fainter than at peak in B. A few objects which have been observed for a longer period show that the decline slows down to 0.014mag/day and 0.015mag/day in B and V respectively, at a phase between 120 and 140 days (Leibundgut, 2000).

1.3.3 Cosmology with Ia SNe

In 2011 Saul Perlmutter, Adam Riess and Brian Schmidt received the Nobel Prize in Physics "for the discovery of the accelerating expansion of the Universe through observations of distant supernovae", i.e. for the discovery of a positive cosmological constant ($\Omega_\Lambda > 0$) and a current acceleration of the expansion ($q_0 < 0$) (Riess et al., 1998).

If we look at the difference between the observed maximum brightness of a Ia SNe and the expected value in an empty Universe (Einstein de-Sitter model, Ω_m=Ω_Λ=0), as shown in Figure 1.4 (Riess et al., 2004), we can see, already by considering only supernovae with z $<$ 1, that they are fainter than predicted. By taking into account that an empty Universe would expand at constant rate ($\ddot{a}$= 0), this means that the luminosity distance in such a Universe is therefore larger than in any other Universe with a vanishing cosmological constant. The luminosity distance can only be increased by assuming that the Universe expanded more slowly in the past than it does today, hence that the expansion has accelerated over time, which is only possible possible only if $\Omega_\Lambda > 0$.

This result is consistent with Perlmutter et al. (1999) measurements (Figure 1.5). They have shown that the the high-redshift Ia SNe (z $>$ 1) are brighter than they should be in an empty Universe (Schneider, 2006).

However, there are other possible explanations of the observations which don't require an accelerated expanding Universe. The measurements of cosmological parameters mentioned afore are based under the assumption that all Ia SNe have the same peak luminosity (after correcting for the Phillips relationship), not dependent of their redshift, but a redshift dependent evolution, in such way that Ia SNe at increasing redshift are becoming less luminous at their peak brightness, would have a similar effect on the Hubble diagram as the accelerated expansion of the Universe. A possible reason might be that the Chandrasekhar mass limit, at which the explosion is triggered, may depend on chemical composition of white dwarfs, and this in turn may be redshift dependent. Another uncertainty is due to dust extinction. The correction of the peak luminosity for extinction in host galaxy and in the Milky Way is determined from reddening (see eq. 1.4), which depends on dust

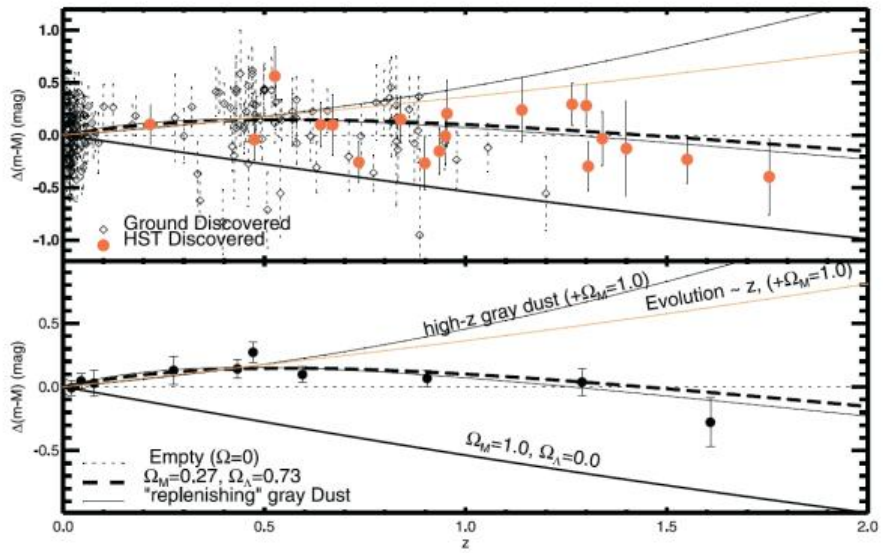

Figure 1.4: Difference between the maximum brightness of SNe Ia and that expected in an empty Universe. Diamond symbols represent events that were detected from the ground, circles the ones discovered by the HST in near-IR wavebands. In the top panel, the individual SNe Ia are presented, whereas in the bottom panel they are averaged in redshift bins. An empty Universe would correspond to the dotted straight line, D(m-M) = 0. The dashed curve corresponds to a cosmological model with Ω_m = 0.27, Ω_Λ=0.73. Source: Riess et al. (2004); Schneider (2006)

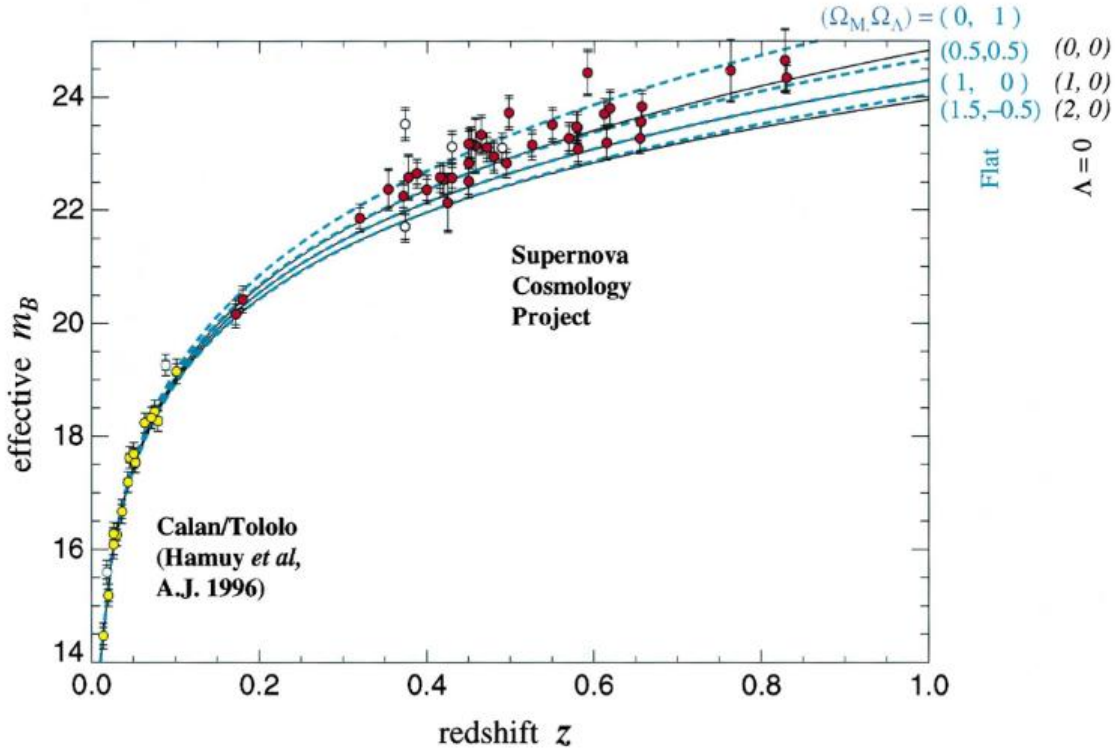

Figure 1.5: Hubble diagram for 42 high-redshift type Ia supernovae from the Supernova Cosmology Project and 18 low-redshift type Ia supernovae from the Supernova Survey, plotted on a linear redshift scale to display details at high redshift. Source: Perlmutter et al. (1999)

properties. If the dust properties evolve with redshift, the determined extinction, and thus the correction, might be systematically wrong. Other possible systematics may be caused by the method of peak brightness correction method (i.e. Phillips relationship), or by the selection effects since intrinsic brighter SNe are more easily detected than the fainter ones (Schneider, 2006).

Chapter 2

Data and models

2.1 KINGFISH sample

The KINGFISH project is an imaging and spectroscopic survey of 61 nearby (d $<$ 30 Mpc) galaxies, including 59 galaxies from the SINGS project, for which dust mass estimates have been determined (Draine et al. (2007); Skibba et al. (2011)). The galaxy sample covers the full range of integrated properties and local interstellar medium environments found in the nearby Universe. Compared to Spitzer, whose limited wavelength coverage makes it difficult to separate dust temperature distributions from grain emissivity functions, Herschel's deep, submillimeter imaging capability at 250, 350, and 500μm with the SPIRE (Spectral and Photometric Imaging Receiver) instrument, enables the direct detection of cool dust and constrains the Rayleigh-Jeans region of the main dust emission components (Kennicutt et al., 2011).

For our purposes, our sample consists of 59 KINGFISH galaxies (Table 2.1). We excluded NGC 1404 and DDO 154 because they lack SPIRE fluxes. The galaxies are grouped according to their morphology: Sa-Sap, Sab-Sbp, Sbc-Scp, Scd-Sdm, S0 and Irregulars, containing 10, 8, 11, 11, 8 and 9 galaxies in the group respectively. NGC3265 is the only elliptical and NGC4625 is a dwarf spiral (SABm). For each galaxy, we created dust mass surface density maps on a pixel by pixel basis. The galaxy distances and heliocentric radial velocities in Table 2.1 are from Kennicutt et al. (2011). The de Vaucouleur radius R_{25} are from the RC3 (de Vaucouleurs et al., 1991). Galaxy types and dust temperatures are from Skibba et al. (2011).

Table 2.1: Sample of the KINGFISH galaxies

Group	GALAXY	TYPE	v	Distance	R_{25}	T_{dust}	*This work* $logM_{dust}$	*Skibba* $logM_{dust}$	*Draine* $logM_{dust}$	*Gordon* $logM_{dust}$
			(kms^{-1})	(Mpc)	$(arcmin)$	(K)	$(logM_{\odot})$	$(logM_{\odot})$	$(logM_{\odot})$	$(logM_{\odot})$
	(1)	(2)	(3)	(4)	(5)	(6)	(7)	(8)	(9)	(10)
Sa-Sap	NGC 1482	Sa	1655	22.6	1.3	31.8 ± 0.9	7.13 ± 0.04	7.13 ± 0.08	7.47	7.43
	NGC 1512	SBa	896	14.35	4.5	20.9 ± 0.8	7.11 ± 0.17	7.0 ± 0.08	7.21	6.96
	NGC 2798	SABap	1726	25.8	1.3	34.9 ± 1.1	6.87 ± 0.07	6.83 ± 0.08	7.29	7.22
	NGC 2841	SABa	638	14.1	4.1	22.1 ± 0.4	7.44 ± 0.07	7.34 ± 0.08	7.74	7.44
	NGC 3351	SBa	778	9.8	3.7	25.6 ± 0.6	6.91 ± 0.09	6.87 ± 0.08	7.46	7.32
	NGC 3190	SAap	1271	19.3	2.2	25.2 ± 0.5	6.97 ± 0.12	6.89 ± 0.08	7.19	7.11
	NGC 4579	SBa	1519	15.3	2.9	23.4 ± 0.5	7.19 ± 0.06	7.12 ± 0.08	8.18	7.77
	NGC 4594	SAa	1091	9.4	4.4	22.1 ± 0.4	6.99 ± 0.07	6.91 ± 0.08	7.56	7.56
	NGC 4725	SABa	1206	12.7	5.4	21.1 ± 0.4	7.41 ± 0.09	7.34 ± 0.08	8.2	7.88
	NGC 4736	SABa	308	4.66	5.6	29.3 ± 0.8	6.55 ± 0.09	6.52 ± 0.08	7.11	6.97
Sab-Sbp	NGC 1097	SBabp	1275	19.09	4.7	26.2 ± 0.6	7.86 ± 0.06	7.8 ± 0.08	8.37	8.05
	NGC 2146	SBabp	893	17.2	3.0	37.4 ± 1.2	7.45 ± 0.04	7.36 ± 0.08	…	…
	NGC 3049	SBab	1494	19.2	1.1	27.5 ± 0.7	6.55 ± 0.06	6.45 ± 0.08	6.74	6.62
	NGC 3627	SBbp	727	10.3	4.6	27.2 ± 0.7	7.38 ± 0.05	7.32 ± 0.08	7.69	7.61
	NGC 4569	SABab	-235	15.3	4.8	24.0 ± 0.5	7.22 ± 0.17	7.16 ± 0.08	7.75	7.67
	NGC 4826	SAab	408	5.57	5.0	29.1 ± 0.8	6.5 ± 0.09	6.38 ± 0.08	6.89	6.77
	NGC 5713	SBabp	1883	21.37	1.4	30.0 ± 0.8	7.15 ± 0.04	7.07 ± 0.08	7.95	7.7
	NGC 7331	SAb	816	14.9	5.2	26.1 ± 0.6	7.82 ± 0.05	7.71 ± 0.08	8.05	7.99
Sbc-Scp	NGC 628	SAc	657	7.3	5.2	24.0 ± 0.6	7.09 ± 0.07	7.03 ± 0.08	8.02	7.58
	NGC 3184	SAbc	592	8.7	3.7	23.4 ± 0.5	6.95 ± 0.06	6.9 ± 0.08	7.7	7.15
	NGC 3198	SABbc	663	14.5	4.3	23.6 ± 0.5	7.26 ± 0.09	7.18 ± 0.08	7.42	7.07
	NGC 3521	SABbc	805	12.44	5.5	24.9 ± 0.6	7.71 ± 0.05	7.63 ± 0.08	7.83	7.7
	NGC 3938	SAc	809	12.1	2.7	24.8 ± 0.5	7.03 ± 0.05	6.94 ± 0.08	7.69	7.37
	NGC 4254	SAcp	2407	15.3	2.7	25.5 ± 0.5	7.57 ± 0.02	7.56 ± 0.08	8.55	8.16
	NGC 4321	SABbc	1571	15.3	3.7	24.4 ± 0.5	7.64 ± 0.03	7.61 ± 0.08	8.57	8.22
	NGC 4536	SABbc	1808	15.3	3.8	26.9 ± 0.6	7.31 ± 0.07	7.28 ± 0.08	7.8	7.85
	NGC 5055	SAbc	504	10.16	6.3	24.1 ± 0.5	7.69 ± 0.05	7.61 ± 0.08	8.19	7.87
	NGC 5457	Sc	241	7.1	14.4	24.3 ± 0.6	7.64 ± 0.1	7.52 ± 0.08	…	…
	NGC 7793	SAc	230	3.91	4.7	24.1 ± 0.6	6.58 ± 0.05	6.51 ± 0.08	6.92	6.52
Scd-Sdm	IC 342	SABcd	31	3.28	10.7	24.1 ± 0.6	7.25 ± 0.03	7.27 ± 0.05	…	…
	NGC 337	SABcdp	1650	22.9	1.4	28.1 ± 0.7	7.13 ± 0.05	7.07 ± 0.08	7.65	7.38
	NGC 925	SABd	553	9.04	5.2	23.7 ± 0.5	7.06 ± 0.08	6.98 ± 0.08	7.35	7.06
	NGC 2976	SABd	3	3.6	2.9	25.9 ± 0.7	6.05 ± 0.06	5.97 ± 0.08	6.34	6.2
	NGC 3621	SAd	727	6.9	6.2	25.4 ± 0.6	7.09 ± 0.09	6.97 ± 0.08	7.38	7.2
	NGC 4236	SBdm	0	3.6	10.9	25.0 ± 0.7	6.23 ± 0.31	5.83 ± 0.08	6.15	5.79
	NGC 4559	SBcd	816	8.45	5.4	24.5 ± 0.5	6.94 ± 0.06	6.83 ± 0.08	7.57	7.24
	NGC 4631	SBd	606	7.62	7.7	27.7 ± 0.8	7.35 ± 0.09	7.26 ± 0.08	8.11	7.68
	NGC 5398	SBdm	1216	8.33	1.4	27.3 ± 0.7	5.71 ± 0.15	5.59 ± 0.08	…	…
	NGC 5474	SAcd	273	6.8	2.4	24.6 ± 0.6	6.06 ± 0.14	6.0 ± 0.08	6.39	6.06
	NGC 6946	SABcd	48	6.8	5.7	26.0 ± 0.6	7.49 ± 0.03	7.47 ± 0.08	7.74	7.52
S0	NGC 584	SAB0	1854	20.8	2.1	24.5 ± 0.6	6.27 ± 0.77	5.58 ± 0.15	…	…
	NGC 855	SA0	610	9.73	1.3	28.5 ± 0.9	5.56 ± 0.27	5.49 ± 0.08	5.69	5.57
	NGC 1266	SB0	2194	30.6	0.8	36.0 ± 1.0	6.7 ± 0.06	6.66 ± 0.08	7.05	7.27
	NGC 1291	SAB0	839	10.4	4.9	22.4 ± 0.5	6.8 ± 0.32	6.76 ± 0.08	7.34	7.29
	NGC 1316	SAB0	1760	20.1	6.0	26.8 ± 0.7	7.04 ± 1.64	6.79 ± 0.08	7.63	7.67
	NGC 1377	S0	1792	24.6	0.9	43.5 ± 1.8	5.95 ± 0.16	5.78 ± 0.09	…	…
	NGC 3773	SA0	987	12.4	0.6	30.2 ± 0.8	5.46 ± 0.09	5.44 ± 0.08	5.9	6.0
	NGC 5866	S0	692	15.3	2.4	27.9 ± 0.7	6.68 ± 0.17	6.57 ± 0.08	6.65	6.84
Irregulars	DDO 53	Im	19	3.6	0.8	30.5 ± 0.9	3.87 ± 0.33	4.01 ± 0.10	4.0	4.35
	DDO 165	Im	37	3.6	1.7	23.5 ± 1.1	4.48 ± 0.33	4.19 ± 0.10	…	…
	Ho I	IABm	143	3.6	1.8	26.2 ± 0.9	4.42 ± 0.42	4.54 ± 0.08	4.83	4.61
	Ho II	Im	157	3.6	4.0	36.5 ± 1.1	5.08 ± 0.89	4.05 ± 0.20	5.07	5.38
	IC 2574	IBm	57	3.6	6.6	25.9 ± 0.6	5.93 ± 0.32	5.57 ± 0.08	5.86	6.04
	M81dwB	Im	350	3.6	0.4	25.0 ± 0.7	3.61 ± 0.28	4.06 ± 0.09	…	…
	NGC 2915	I0	468	3.78	0.9	28.9 ± 0.9	4.61 ± 0.16	4.59 ± 0.08	4.14	3.77
	NGC 3077	I0p	14	3.6	2.7	30.1 ± 0.9	5.67 ± 0.07	5.52 ± 0.08	…	…
	NGC 5408	IBm	509	4.8	0.8	25.7 ± 1.1	4.66 ± 0.23	4.68 ± 0.08	4.67	4.09
	NGC 3265	E	1421	19.6	0.6	31.8 ± 0.9	5.92 ± 0.07	6.0 ± 0.08	6.17	6.28
	NGC 4625	SABm	609	9.3	1.1	24.8 ± 0.6	5.84 ± 0.08	5.89 ± 0.08	6.35	6.18

Notes. The galaxy morphological types (2), heliocentric radial velocities (3) and galaxy distances (4) were taken from Table 1 in Skibba et al. (2011). They obtained the morphological types from Buta et al. (2010) and Kennicutt et al. (2003). The de Vaucouleur's radii R_{25} (5) were calculated from RC3 D_{25} diameters (de Vaucouleurs et al., 1991). The global dust temperatures (6) were determined by Skibba et al. (2011). The dust mass in column (7) is our integrated dust mass within 1 R_{25}. Dust masses in column (8) were determined by Skibba et al. (2011), in column (9) by Draine et al. (2007) for SINGS, and in column (10) by Gordon (2008) for SINGS, and are listed for comparison purposes.

2.2 Dust mass maps

Skibba et al. (2011) calculate the total dust mass for each KINGFISH galaxy under the assumption that the dust radiates as a blackbody:

$$\mathrm{M_{dust}} = \frac{f_\lambda 4\pi \mathrm{D}^2}{\kappa_{\mathrm{abs},\lambda} 4\pi \mathrm{B}_\lambda(\mathrm{T_{dust}})}, \tag{2.1}$$

where $f_\lambda = f_\nu \mathrm{c}/\lambda^2$ is the flux density, D, the distance to the galaxy, κ_{abs} is the mass absorption coefficient and $B_\lambda = 2\mathrm{c}k_B\mathrm{T}/\lambda^4$ is the Planck function in the Rayleigh-Jeans limit. They determine the dust temperature by fitting a single temperature blackbody curve to the *Spitzer* MIPS and *Herschel* SPIRE FIR and submm flux densities, assuming a dust emissivity $\epsilon \propto \lambda^{-\beta} B_\lambda(T_{dust})$, with β=1.5. Temperature uncertainties are determined from

a Monte Carlo analysis that includes the flux errors. Dust masses are calculated using the standard Milky Way dust model with R_V = 3.1 (Weingartner and Draine, 2001), and $\kappa_{abs,500\mu m}$ = 0.95 $cm^2 g^{-1}$ (Draine, 2003a). Dust masses are computed at 500μm to minimize the temperature dependence, although the flux uncertainties are larger than at short wavelengths, where the estimated masses are lower (Skibba et al., 2011).

We create dust mass surface density maps (shown in Appendix A) on a pixel-by-pixel basis using equation 2.1, the Skibba et al. (2011) global dust temperatures and the Herschel Interactive Processing Environment (HIPE) processed, background subtracted 500μm maps (Kennicutt et al., 2011). SPIRE maps have wavelength dependent pixel scales; at 500μm it is 14 arcsec/pixel. We convert map fluxes from MJy/sr to MJy/parsec using the distances in Skibba et al. (2011).

As a cross-check, we integrated the mass over all the pixels within the de Vaucouleur's radius R_{25}, and compared them to values in Skibba et al. (2011). On average, our integrated masses are 18 $\pm$ 26 $\%$ larger, with the exception of NGC 4236 and NGC 584 where they are 4 and 10 times larger. A source for the difference is that Skibba et al. (2011) used 3.6 μm images to create elliptical apertures for the photometry, which were chosen to approximately encompass all of the optical and infrared emission of the galaxy, while we integrated the mass within a circle of R_{25}, and thereby over a larger area. For face-on galaxies our integrated mass is within a few percent of that calculated by Skibba et al. (2011). Our dust masses in NGC1482, NGC2915, NGC3773, NGC4254, NGC5408, NGC6946, IC0342 are consistent within 5$\%$ with Skibba's masses. All the galaxies have similar sizes of minor to major axes. Another source might be that they used differently processed Herschel maps, with slightly different background subtraction or calibration. The HIPE reduced maps have 15-20$\%$ negative pixel values, which we set to zero.

Our results are in column 7 of Table 2.1. Note that errors are statistical errors due to the dust temperature and 500μm flux uncertainties, and do not include systematic uncertainties. In column 9 of Table 2.1 we list dust masses determined by Draine et al. (2007) from the SINGS data, which are $\sim$2-3 times larger than larger than Skibba's. These were calculated assuming a multi-temperature dust model consisting of a mixture of different grain types with a distribution of grain sizes.

In column 10 we list dust masses for SINGS galaxies estimated by Gordon (2008) from the 70 micron to 160 micron flux ratio, assuming the dust radiates as a black body whose emissivity is proportional to λ^{-2}. He used a single dust temperature, estimated from the flux ratio, which combined with the measured 160 micron surface brightness and a simple, homogeneous dust grain model consisting of 0.1 micron silicon grains with the standard grain emissivity at 160 microns, provides the dust mass (cf. Gordon et al. (2010)). Dust masses obtained in this manner are $\sim$ 2 times larger than ours, but smaller than Draine et al.'s (2007). The influence of the total dust mass uncertainty on the results is discussed in §4.3.

2.3 Dust model and extinction law

The amount of extinction depends on wavelength, the dust mass surface density, and the dust model. Extinction can be calculated from

$$\mathrm{A}_\lambda = [(\mathrm{A}_\lambda/\mathrm{N_H})(\mathrm{M_H}/\mathrm{M_{dust}})/\mathrm{m_H}]\sigma_{\mathrm{dust}}, \tag{2.2}$$

and the extinction in V is

$$A_V = [(A_V/N_H)(M_H/M_{dust})/m_H]\sigma_{dust},$$

where σ_{dust} is the dust mass surface density, N_H the H column density, m_H is the mass of a hydrogen atom, and A_V/N_H is the attenuation per unit column density. The Milky Way R_V = 3.1 dust models of Weingartner and Draine (2001) have A_V/N_H = 5.3×10^{-22} mag cm^2 H^{-1}, and a gas-to-dust mass ratio M_H/M_{dust} = 98.0392 (see Table 3 in Draine et al. (2007)).

We apply the Cardelli, Clayton, and Mathis (1989) (hereafter CCM) extinction law to calculate the extinction curve:

$$\frac{\mathrm{A}(\lambda)}{\mathrm{A(V)}} = \mathrm{a(x)} + \mathrm{b(x)}/\mathrm{R_V} \tag{2.3}$$

where a(x) and b(x) are wavelength dependent coefficients given in CCM.
At infrared wavelengths, 0.3 $\mu m^{-1} \leq$ x $\leq 1.1 \mu m^{-1}$:

$$\mathrm{a(x)} = 0.574\mathrm{x}^{1.61} \qquad and \qquad \mathrm{b(x)} = -0.527\mathrm{x}^{1.61}$$

and in the visible/NIR, 1.1 $\mu m^{-1} \leq$ x $\leq 3.3 \mu m^{-1}$:

$$\begin{aligned} a(x) = 1 + 0.17699y - 0.50447y^2 - 0.02427y^3 + \\ +0.72085y^4 + 0.01979y^5 - 0.77530y^6 + 0.32999y^7 \end{aligned}$$

and

$$\begin{aligned} b(x) = 1.4138y + 2.28305y^2 + 1.07233y^3 - 5.38434y^4 + \\ -0.62251y^5 + 5.30260y^6 - 2.09002y^7 \end{aligned}$$

where y=(x-1.82) and x=1/λ.

2.4 Spectral templates of type Ia Supernovae

We use the Hsiao et al. (2007) restframe SNe Ia spectra and light curve templates because they are most complete in temporal and wavelength coverage. The multi-epoch spectral templates range from -20 days before B_{max} to 80 days after B_{max}, and were constructed by averaging a large number of observed spectra of nearby SN Ia between 0.1 and 2.5 microns. We tested the Nugent et al. (2002) Type Ia Branch-normal templates, and find that they produce similar results.

Chapter 3

Methods

In this section we describe our Monte Carlo simulation in which we randomly place SNe Ia spectrum templates in KINGFISH galaxies and calculate the dust affected spectrum. The main goal of our Monte Carlo simulation is to create probability plots of SNe Ia color excess as a function of galactocentric distance, and to place uncertainties on the color excess for different galaxy morphology types. We then compare our model to observed spectra of SNe Ia in the KINGFISH galaxies. Finally, we use the generated statistics in the Monte Carlo simulation to determine the absorption-to-reddening ratio R_V of dust in host galaxies of a different sample of observed Ia SNe.

3.1 Statistics with KINGFISH sample

To develop color excess statistics we first investigate the relationship between the SNe dust extinction probability and position in the host galaxy. We also look for differences of the effect of dust extinction in galaxies with different morphological classifications. Our procedure was as follows.

The first step was to randomly place the peak brightness template spectrum 100000 times in each of our KINGFISH galaxies, within a radius of 2 R_{25}. We assume a peak absolute magnitude M_B = -19.5 mag (Saha et al., 1999). The template supernovae are redshifted, and recalculated to observer's frame using the galaxy distances in Table 2.1. The random parameters are projected (*x,y*) centered on the galaxy nucleus, and *ext*, a parametrization of the extinction, corresponding to the fraction of the total amount of dust along the line of sight. A SN in front of the galaxy would have *ext*=0, one behind the galaxy *ext*=1. For each instance, we calculate A_V from equation (2) multiplied by *ext*, and apply the CCM extinction law with R_V = 3.1 to calculate A_λ/A_V, thus determining the selective extinction with λ, which, we then subtract from the SN Ia template. In the second step we calculate the observed (B-V) colors, by convolving Bessel B and V filter passbands (Bessell, 1990) with the extincted SN spectrum. The unreddened, intrinsic $(B-V)_{intrinsic}$ = -0.06 mag is calculated from the template spectrum with the same B and V passbands (A_V = 0 mag). The outputs are $(B-V)_{observed}$, the color excess $E(B-V) = (B-V)_{observed} - (B-V)_{intrinsic}$, and the projected galactocentric distance in pixels. In Figure 3.1 we show the distribution of E(B-V) probability with projected R/R_{25} for each galaxy group. E(B-V) peaks near the center, and decreases with radius, as expected, although peak E(B-V) is highest for Sab-Sb types and lowest for S0 and Irregulars.

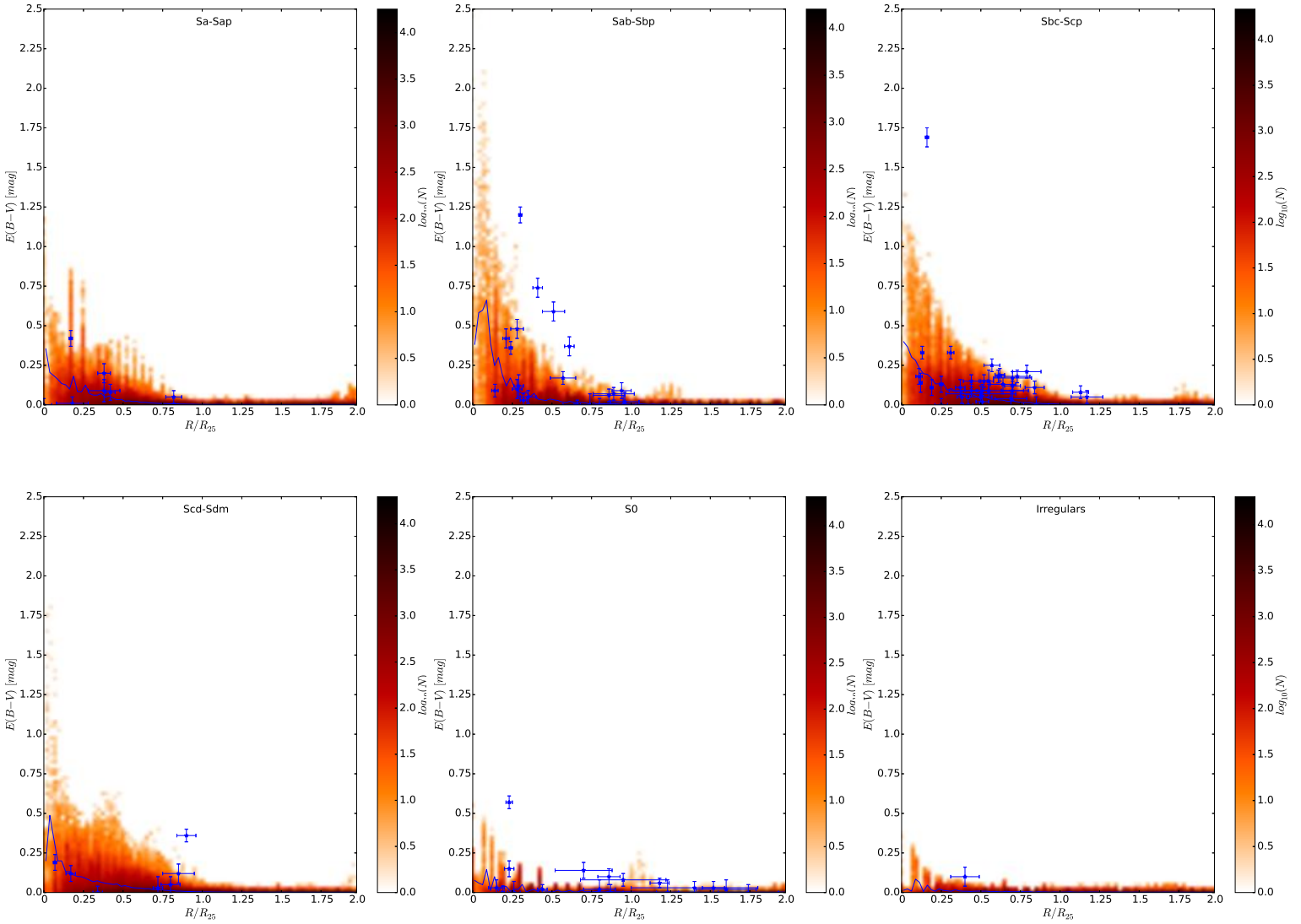

Figure 3.1: E(B-V) vs. normalized galactocentric distance probability plots for each of the galaxy groups: Sa-Sap, Sab-Sbp, Sbc-Scp, Scd-Sdm, S0 and Irregulars. The logarithmic color scale indicates the probability that a SN at a certain distance will have a certain color excess E(B-V), dark for high probability, and bright for low probability. The blue crosses indicate observed SNe Ia from the Wang et al. (2006) sample. The blue lines are weighted means of E(B-V) for bins of size 0.025 R/R_{25}.

3.2 Comparison with observed SNe Ia in KINGFISH galaxies

There are 15 SNe Ia that occurred in KINGFISH galaxies (Table 3.1). We found spectra for five SNe in the online Supernova Spectrum Archive (SUSPECT)[1]: SN 1981B in NGC 4536, SN 1989B in NGC 3627, SN 2002bo in NGC 3190, SN 2006X in NGC 4321 and SN 1966J in NGC 3198. The spectrum of SN 1966J is digitized from a photographic plate, obtained with the prismatic nebular spectrograph on the Crossley reflector at the Lick Observatory. It is valuable for classification purposes, but as the flux is not properly calibrated (Casebeer et al., 2000) it is not useful for our purpose. The units of the SN 1981B spectra

[1] `http://www.nhn.ou.edu/~suspect/`

are unknown, and do not agree with commonly used units by Branch (e.g. in Branch et al. (1983, 1981)). General information about SN 1989B, SN2002bo and 2006X are summarized in Table 3.2.

Having calculated the dust mass in each galaxy pixel, we compare the simulation results to the observed spectra of these historical SNe to see if we can reproduce the observed quantities for R_V=3.1.

The procedure of the comparison is as follows:

1. Match the RA and Dec of the observed SN Ia to the (X,Y) coordinates of the KINGFISH map of the host galaxy.
2. Calculate the extinction curves using R_V=3.1 for different A_V, from 0 to 3.5 in 0.1 steps
3. A_V in the preceeding step are applied to the corresponding restframe template spectra, generating 35 reddened spectra for each epoch.
4. Each spectrum is redshifted into the observer's frame and the appropriate Milky Way extinction applied.
5. The observed and redshifted templates are convolved with the Subaru intermediate filter passbands (Figure 3.2, Taniguchi (2004)) in order to have a number of photometric comparison points.
6. To determine A_V that best matches the observed spectra we apply the least square test,
$$\chi^2 = \mathrm{R}^2 = \sum [\mathrm{OBS_i} - \mathrm{SIM_i}]^2, \tag{3.1}$$
where OBS_i and SIM_i are the observed and simulated photometry in the Subaru filters.
7. To calculate E(B-V), the best matching template spectra are convolved with Bessel B and V filter passbands (Bessell (1990), Figure 3.2) and using $(B-V)_{instrinsic}$ calculated for each epoch.
8. We compare the best fit A_V, to the calculated A_V from the dust assuming ext=1.
9. We also calculate a set of model spectra using different values of R_V (from 0.5 to 5.5 in 0.1 steps), which we then compare to the observed spectra as described in steps 2-7. The results are shown in Table 3.3, and all plots in Appendix B.

3.2.1 SN 1989B in NGC 3627

SN 1989B is a normal SNe Ia which occurred in a bright spiral arm of NGC 3627, 15"W and 50"N of its nucleus. Figure 3.3 shows the position of the SN in the dust mass surface density map, compared to optical SDSS and *Hubble Space Telescope* images. Wells et al. (1994) observed maximum light in B at a magnitude of B = 12.34 $\pm$ 0.05 mag and derived a color excess of E(B-V) = 0.37 $\pm$ 0.03 mag from UBVRIJHK photometry, using Galactic reddening $E(B-V)_{Gal}$=0.032 mag. We simulated the spectra for days 0, 6, 11, 21, 22, 32 and 52, assuming a distance of 11.07 Mpc and an absolute brightness of M_B(max)=-19.48 mag (Saha et al., 1999). The total dust extinction, calculated from the KINGFISH dust mass column density map of NGC 3627, in V band at the position of SN 1989B is A_V

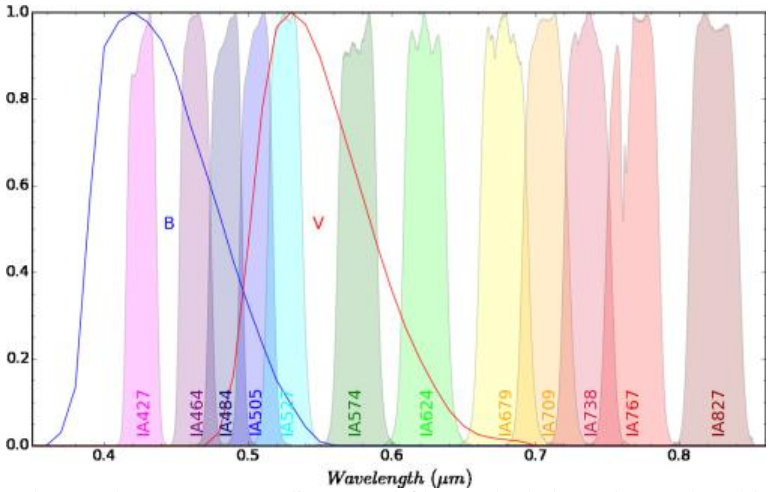

Figure 3.2: Subaru Telescope Intermediate Band filters (shaded), and Bessel B (blue line) and V (red line) filters.

Table 3.1: Overview of Ia SNe in the KINGFISH sample

SN	Host galaxy	Mag.	Type	Spectra
SN 1957A	NGC 2841	14.0	Ia-p	
SN 1966J	NGC 3198	13.0	Ia	SUSPECT
SN 1980N	NGC 1316	12.5	Ia	
SN 1981B	NGC 4536	12.3	Ia	SUSPECT
SN 1989B	NGC 3627	13.0	Ia	SUSPECT
SN 1989M	NGC 4579	12.2	Ia	
SN 1994ae	NGC 3370	15.4	Ia	
SN 1999by	NGC 2841	15.0	Ia-p	
SN 2002bo	NGC 3190	15.5	Ia	SUSPECT
SN 2002cv	NGC 3190	19.0	Ia	
SN 2006dd	NGC 1316	15.0	Ia	
SN 2006mr	NGC 1316	15.6	Ia	
SN 2006X	NGC 4321	17.0	Ia	SUSPECT
SN 2007on	NGC 1404	14.9	Ia	
SN 2011iv	NGC 1404	12.8	Ia	

Notes. Magnitudes and type were taken from the IAU Central Bureau for Astronomical Telegrams (CBAT) (`http://www.cbat.eps.harvard.edu/lists/Supernovae.html`).

= 3.0 mag, in case of *ext*=1, when all of dust is taken into account (σ_{dust}=9.667$\times 10^{-5} g\ cm^{-2}$).

We derive from the simulated best fit spectra E(B-V) = 0.27 $\pm$ 0.07 mag and A_V = 0.95 $\pm$ 0.19 mag in case of applying an extinction law with R_V = 3.1. Figure 3.4 shows the best fitted simulated spectrum to the observed spectra (Barbon et al., 1990) at peak brightness. The results are consistent with the Wells et al. (1994) observations. The amount of dust at

Table 3.2: General information on SN 1989B, SN2002bo and 2006X

SUPERNOVA	GALAXY	DISTANCE (Mpc)	M_B(max) (mag)	B_{mag} (mag)	$E(B-V)_{Gal}$ (mag)	SPECTRA EPOCH RELATIVE TO B$_{max}$	SPECTRUM REFERENCES
SN 1989B	NGC 3627	11.07[1]	-19.48[1]	12.34(0.05)	0.032	0, 6, 11, 21, 22, 31, 52	Barbon et al. (1990)
SN 2002bo	NGC 3190	21.6[2]	-19.41[2]	14.06(0.06)	0.027	-4, -3, -1, 4, 28	Benetti et al. (2004)
SN 2006X	NGC 4321	15.2[3]	-19.1[4]	15.41(0.01)	0.026	-6, 0, 2, 6, 8, 12, 13	Yamanaka et al. (2009)

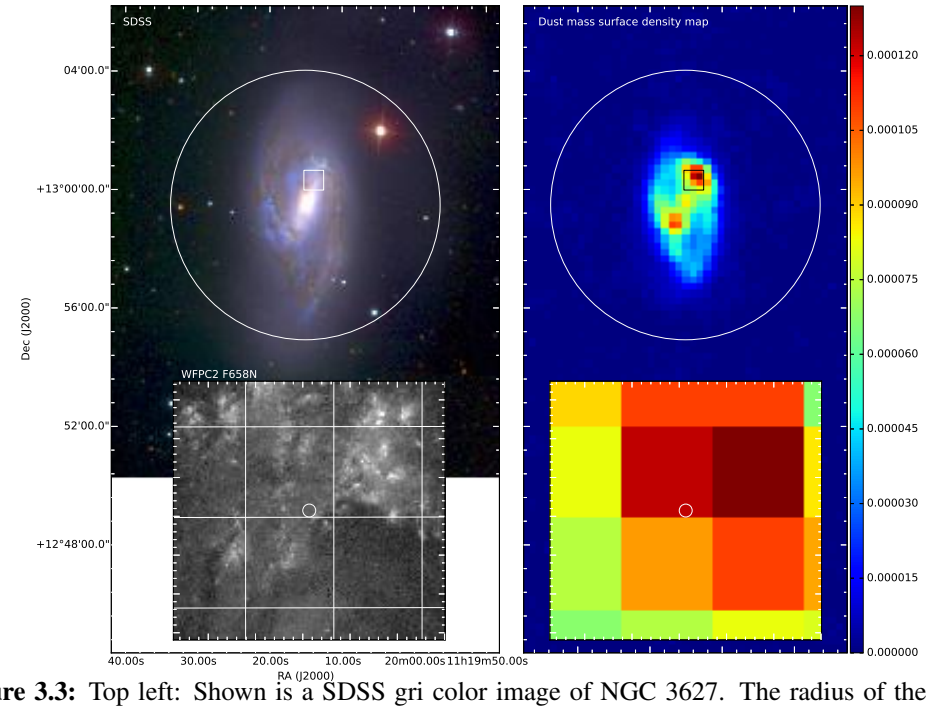

Figure 3.3: Top left: Shown is a SDSS gri color image of NGC 3627. The radius of the white circle corresponds to the de Vaucouleur radius R_{25}. Bottom left: A *Hubble Space Telescope* WFPC2/F658N image of the region inside the white box. The small white circle denotes the position of SN 1989B. The radius of 1" corresponds to the position uncertainty. The gird corresponds to pixels of the Herschel's 500μm map. Top right: Dust mass surface density map of NGC 3627. The region inside the black box is shown enlarged bottom right. The white circle denotes the position of the SN, in a high dust density region.

the location where SN 1989B occurred is enough to cause the observed reddening.

We vary the R_V value, and apply the extinction law until the simulated spectrum best fits the observed ones. We derive an average absorption-to-reddening ratio R_V = 3.16 $\pm$ 1.54 mag and E(B-V)= 0.34 $\pm$ 0.21 mag from observed spectra at seven different epochs. The results are given in Table 3.3, and Figure 3.5 shows of the best fit simulated spectrum to the observed spectra (Barbon et al., 1990) at peak brightness.

3.2.2 SN 2002bo in NGC 3190

SN 2002bo is a typical branch normal type Ia SN at visible and infrared wavelengths. Benetti et al. (2004) determined its peak absolute magnitude M_B(max) = -19.41 mag, E(B-V) $\sim$ 0.47 mag and a distance of 21.6 Mpc. Milky Way extinction along the line of sight is E(B-V)$_{Gal}$ = 0.027 mag (Schlegel et al., 1998). The dust mass column density in the KINGFISH dust maps at the position of SN 2002bo is σ_{dust}=(3.155$\pm$0.112)$\times 10^{-5} g\ cm^{-2}$, corresponding to A_V = 0.98 $\pm$ 0.04 mag.

For R_V = 3.1, we find that the best fitting template to the observed spectra have A_V = 1.34 $\pm$ 0.19 mag and E(B-V)= 0.41 $\pm$ 0.07 mag. This A_V value is significantly larger ($\sim$ 35%) than the value calculated from the Herschel derived dust masses. Possible reasons for this discrepancy are:

a) Dust mass uncertainty - total dust masses for this galaxy range from $10^{6.89} M_\odot$ (determined by Skibba) to $10^{7.19} M_\odot$ (determined by Draine). Our total integrated mass of $10^{6.97} M_\odot$ is $\sim$66% lower than the Draine et al. (2007) mass, and $\sim$38% lower than the Gordon (2008) mass.

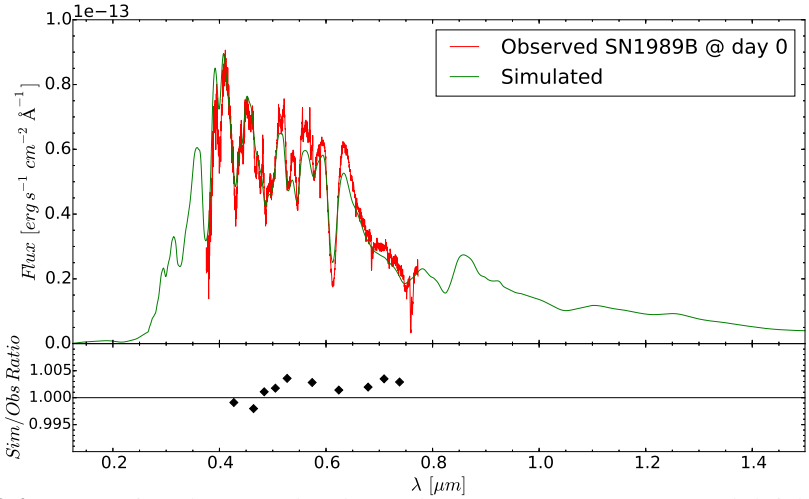

Figure 3.4: Comparison between the observed SN 1989B spectrum at peak brightness and the spectral template, for R_V = 3.1. The template best matches the observed spectrum after applying CCM extinction law with A_V = 1.2 mag. The apparent brightness at maximum light of the simulated best fit spectrum is m_B = 12.46 mag, and E(B-V) = 0.37 mag, which is consistent with the observations. The bottom plot shows the ratio between simulated and observed fluxes calculated by convolving the spectra with Subaru Telescope Intermediate Band filters.

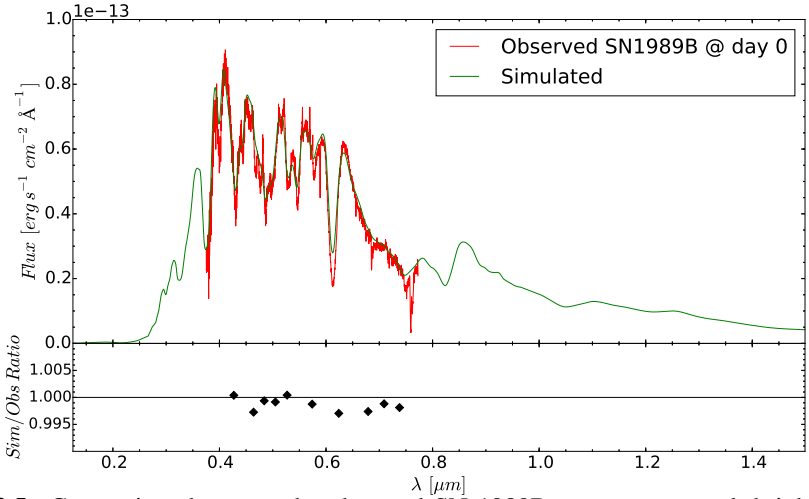

Figure 3.5: Comparison between the observed SN 1989B spectrum at peak brightness and the spectral template. The best fit spectrum is obtained by applying the extinction law with R_V = 2.2 and A_V = 1.1 mag. The apparent brightness at maximum light of the simulated best fit spectrum is m_B = 12.48 mag, and E(B-V) = 0.48 mag. The bottom plot shows ratios between simulated and observed fluxes calculated by convolving the spectra with Subaru Telescope Intermediate Band filters.

b) $R_V \neq 3.1$ - we recalculate the template spectra using different values of R_V = 0.5-5.5 in 0.1 steps, varying A_V between 0 and 3.5 in 0.1 steps for each R_V. We find the best fit R_V = 3.24 $\pm$ 0.97, and E(B-V) = 0.41 $\pm$ 0.07 mag, which is comparable to R_V = 3.1. Figure 3.6 shows a least square colormap for best fit determination of the template to the observed spectra 4 days before peak brightness. Figure 3.7 shows the observed Benetti et al. (2004) spectra and our best fit computed spectrum for day -1 relative to maximum

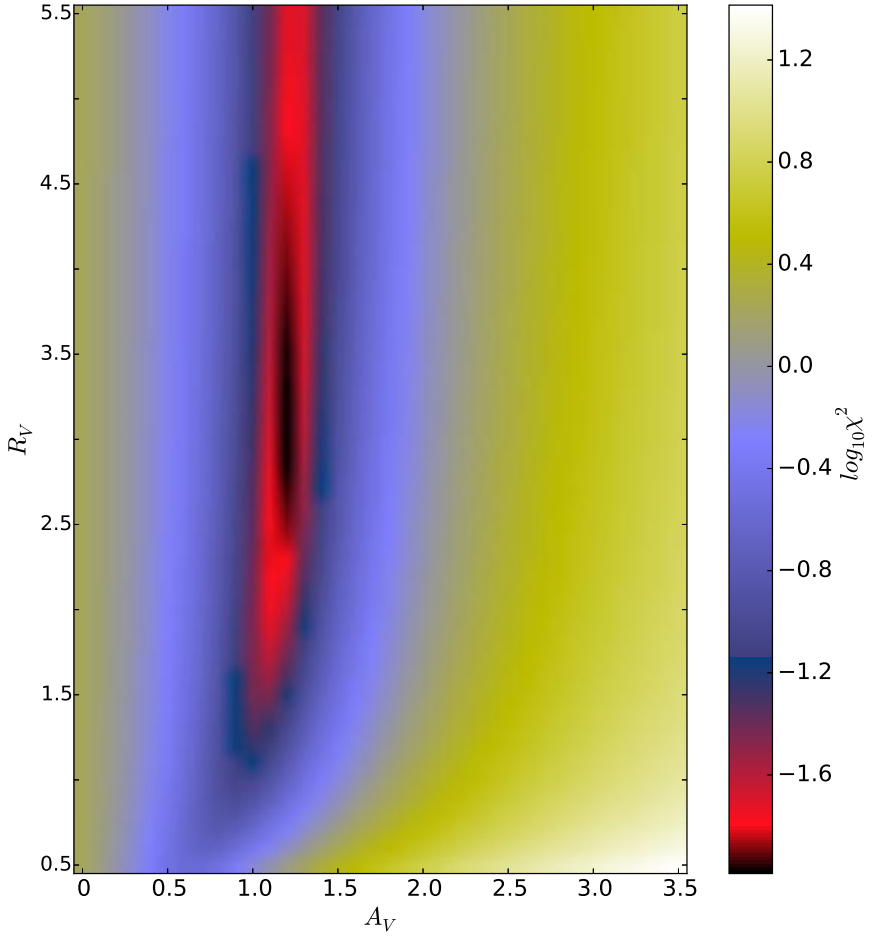

Figure 3.6: The distribution of χ^2 values for the matching procedure for SN 2002bo, 4 days before peak brightness. We apply an extinction law with a range of different R_V and A_V values to the spectrum template, and calculate χ^2 using observed and simulated Subaru intermediate passbands photometry. In this case, the template best matches the observed spectrum after applying the extinction law with R_V = 3.1 and A_V = 1.2 mag. However, the difference in χ^2 for $R_V \sim$ 2.7 - 3.3, at A_V = 1.2 mag is very small.

brightness.

c) if the dust is clumpy, not homogeneously distributed - at NGC 3190 distance, Herschel 500μm pixel corresponds to $\sim$1.45 kpc. Figure 3.8 shows a *Hubble Space Telescope* ACS/WFC (PropID: 10594) composite image of NGC 3190 with the position of SN 2002bo and the 500μm SPIRE map pixel marked. SN 2002bo is inside a spiral arm of NGC 3190 surrounded with clumpy dust features (ACS image), and the dust is not smoothly distributed within the SPIRE pixel. If SN 2002bo lies within a dust clump, this may explain the larger observed extinction compared to the average A_V value calculated for the 500μm pixel. The ratio between WFPC2/F336W (PropID: 11966) and ACS-WFC/F814W also shows that the dust is not smoothly distributed near SN 2002bo.

3.2.3 SN 2006X in NGC 4321

According to Wang et al. (2008a), SN 2006X is highly reddened by abnormal dust, and compared to other SNe Ia, has a peculiar intrinsic color evolution and the highest expansion velocity ever published for a SN Ia. It seems to have a color excess of E(B-V) $\sim$ 1.42 mag

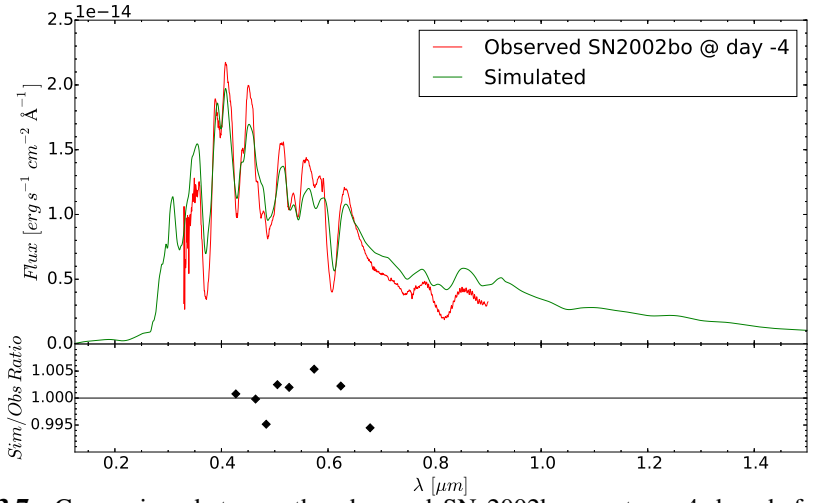

Figure 3.7: Comparison between the observed SN 2002bo spectrum 4 days before maximum brightness and the spectral template. The best fit spectrum is obtained by applying extinction law with R_V = 3.1 and A_V = 1.2 mag. The bottom plot shows ratios between simulated and observed fluxes calculated by convolving the spectra with Subaru Telescope Intermediate Band filters.

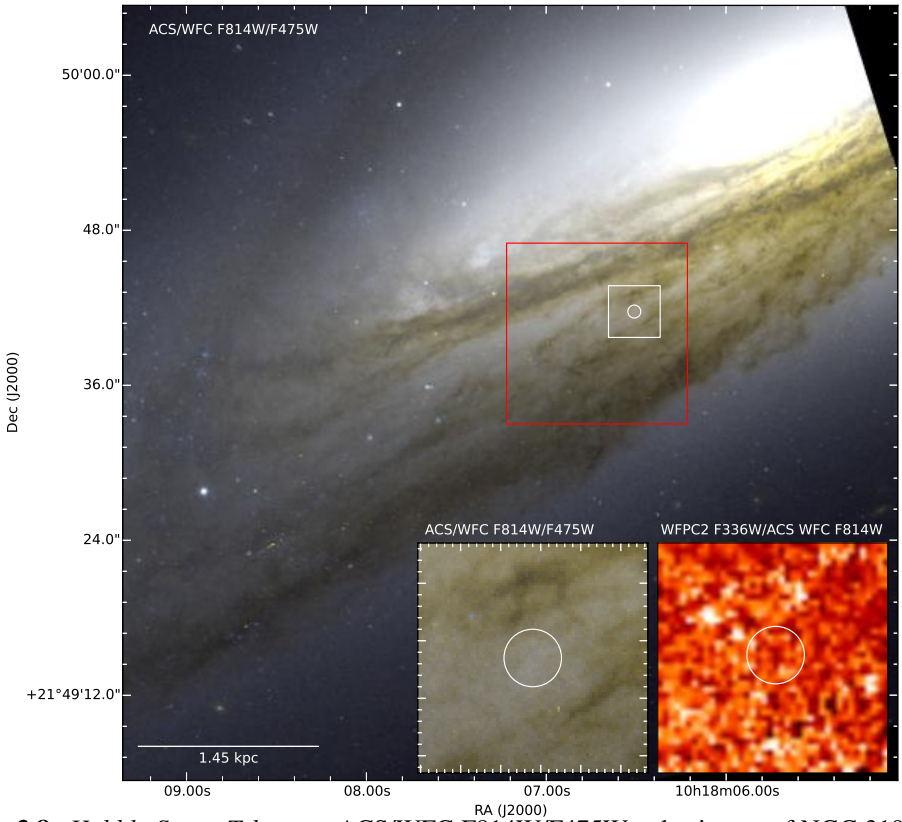

Figure 3.8: *Hubble Space Telescope* ACS/WFC F814W/F475W color image of NGC 3190. The position of SN 2002bo is marked with the small, white circle. The large red square (14" x 14") is the SPIRE map pixel. The region within the small white box is shown enlarged in the two inset figures, where the r = 0.5" circle corresponds to the position uncertainty of the SN. Bottom left: Zoomed in view of the ACS image. Bottom right: WFPC2 F336W - ACS/WFC F814W color map. In both inset images, the clumpy distribution of dust is noticeable.

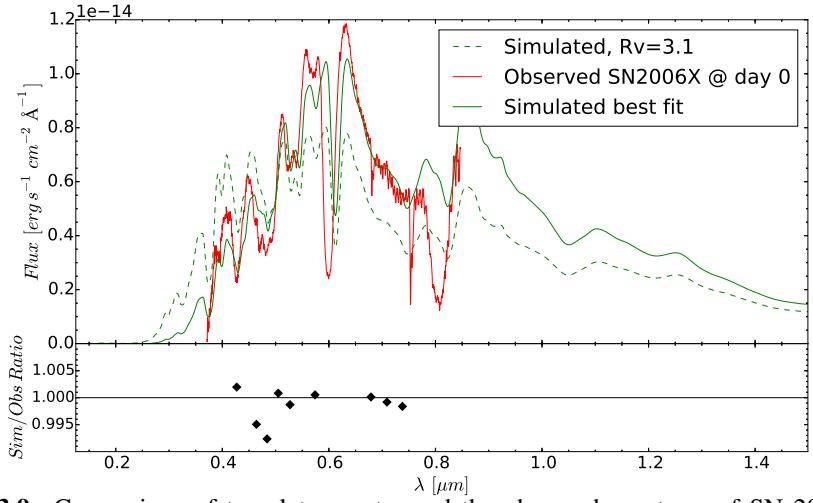

Figure 3.9: Comparison of template spectra and the observed spectrum of SN 2006X at peak brightness. The dashed line is the best fit template with R_V = 3.1, and $A_V = 2.4$ mag. The solid green line is the best fit for an extinction law with R_V = 1.6 and A_V = 2.2 mag.

with $R_V \sim 1.48$ which is much smaller than the Milky Way value of R_V = 3.1, indicating that the dust surrounding SN 2006X has much smaller grain size than typical interstellar dust. They also note that most highly reddened known SNe Ia with $E(B-V)_{Host} >$ 0.5, tend to have R_V values smaller than 3.1, which suggests that dust surrounding some high extinguished SNe may be different from that observed in the galaxy and used in our model. Patat et al. (2009) performed spectropolarimetric analysis and concluded that the dust mixture is significantly different from that typically found in Milky Way, with a lower total to selective extinction ratio R_V than commonly measured in the Milky Way . They suggest that the bulk of extinction is due a molecular cloud.

We used the Cepheid distance to M100 of 15.2 Mpc, and an absolute brightness at peak of M_B = -19.1 mag (Wang et al., 2008b) to best fit the simulated spectra to observations. The visual extinction at the position of SN 2006X in the extinction map of NGC 4321 is A_V = 1.05 mag (for R_V= 3.1). The Milky Way reddening in direction of M100 is $E(B-V)_{Gal}$ = 0.026 mag. We determined from spectra at seven different epochs (Table 3.3) an average R_V = 1.46 $\pm$ 0.29, and E(B-V) = 1.39 $\pm$ 0.05 mag. This R_V ratio is consistent with the values determined by others. The observed spectra of SN 2006X do not fit the computed extinguished spectra with R_V = 3.1 dust (Figure 3.9).

Table 3.3: KINGFISH SNe best fit results. The range is: 0.5 $> R_V >$5.5; 0.0$> A_V >$3.5, step size=0.1

SN NAME	$Epoch$ (day)	BEST FIT R_V	A_V (mag)	$E(B-V)_{Host}$ (mag)	B_{mag} (mag)	$B-V$ (mag)	FIXED R_V=3.1 A_V (MAG)	$E(B-V)_{Host}$ (mag)	B_{mag} (mag)	$B-V$ (mag)
SN 1989B	0	2.2	1.1	0.48	12.48	0.48	1.2	0.37	12.46	0.37
	6	2.5	1.0	0.37	12.47	0.51	1.0	0.29	12.39	0.44
	11	1.1	0.9	0.75	13.18	1.07	1.1	0.32	12.93	0.64
	21	2.9	1.1	0.32	14.03	1.17	1.1	0.30	14.0	1.15
	22	5.4	0.9	0.13	13.73	1.04	0.9	0.24	13.85	1.15
	32	5.5	0.7	0.09	14.26	1.20	0.6	0.15	14.22	1.26
	52	2.5	0.8	0.27	15.17	1.19	0.8	0.21	15.11	1.13
SN 2002bo	-4	3.1	1.2	0.37	14.09	0.29	1.2	0.37	14.09	0.29
	-3	3.0	1.2	0.39	14.04	0.33	1.2	0.37	14.03	0.31
	-1	2.3	1.2	0.51	14.11	0.48	1.3	0.41	14.10	0.38
	4	2.7	1.3	0.46	14.25	0.54	1.3	0.40	14.18	0.48
	28	5.1	1.8	0.31	16.83	1.43	1.7	0.47	16.9	1.59
SN 2006X	-6	1.4	2.0	1.37	15.66	1.29	2.2	0.70	15.17	0.62
	0	1.6	2.2	1.31	15.46	1.30	2.4	0.76	15.10	0.75
	2	0.9	1.4	1.45	14.83	1.48	1.7	0.53	14.19	0.56
	6	1.4	2.1	1.39	15.64	1.52	2.3	0.71	15.15	0.84
	8	1.8	2.7	1.38	16.37	1.57	2.8	0.86	15.94	1.05
	12	1.3	2.2	1.49	16.37	1.84	2.5	0.75	15.91	1.10
	13	1.8	2.8	1.37	16.95	1.76	3.0	0.88	16.65	1.28

Chapter 4

Results & discussion

4.1 Color excess probabilities

As described in §2.1, we divided the galaxies into six groups according to their morphology. For each group, we binned the color excess values and galactocentric distances from the Monte Carlo simulation in bins of 0.025 mag for E(B-V) and 0.025 for normalized galactrocenric distances R/R_{25}. The color excess probability maps are shown in Figure 3.1. The color indicates the number of Ia SNe with a certain E(B-V) value at a certain distance from the galaxy center. The variation in dust mass distribution and amount among galaxy types affects the color excess E(B-V). From our simulation, we expect that the most extinguished SNe will occur in Sab-Sb galaxies, the most dust rich galaxy class, while SNe in S0 and Irregulars are less affected by dust. The blue lines are the mean, i.e. most probable, E(B-V). The blue crosses are observed SNe Ia from Wang et al. (2006) (Table 1 and 2).

We fit the mean color excess values as a function of R/R_{25}:

$$\mathrm{E_{B-V}(R/R_{25})} = f(\mathrm{R/R_{25}}) = \mathrm{a\exp(b(R/R_{25})^{c}}), \tag{4.1}$$

where a, b and c are free parameters determined by the least square method. Figure 4.1 compares the mean E(B-V) to the fitted functions. The parameters and standard deviations for different galaxy types are given in Table 4.1. The most probable extinction A_V can be derived from the color excess functions simply by multiplying by 3.1.

Table 4.1: Color excess function parameters

	$E_{B-V}(R/R_{25}) = a\exp(b(R/R_{25})^c)$		
GALAXY TYPE	a	b	c
Sa-Sap	0.43(0.04)	-3.87(0.16)	0.59(0.05)
Sab-Sbp	0.56(0.03)	-24.91(9.98)	2.02(0.28)
Sbc-Scp	0.45(0.01)	-4.1(0.07)	0.85(0.02)
Scd-Sdm	0.36(0.04)	-4.98(0.8)	1.00(0.16)
S0	0.08(0.01)	-4.6(1.36)	1.11(0.32)
Irregular	0.03(0.01)	-3.34(1.07)	1.30(0.48)

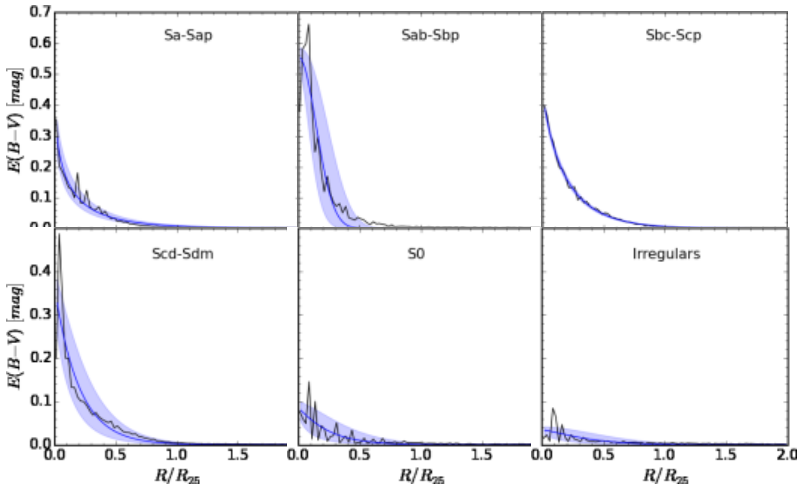

Figure 4.1: Mean E(B-V) values from our Monte Carlo simulation (black line) compared to the fitted $E_{B-V}(R/R_{25})$ functions (eq.4.1, blue line) for different morphological classes. The shaded blue shows the 1-σ uncertainty of the best fit parameters (Table 4.1).

4.2 R_V estimation of host galaxy dust of a SNe Ia sample

We have shown that starting with dust mass values, and R_V = 3.1, we can calculate A_V, and determine the most likely E(B-V). In this section we invert the process, and determine the most likely absorption-to-reddening ratio R_V, given E(B-V).

From the statistical sample of color excesses $E(B-V)_{SIM}$ as a function of galactocentric distance, generated by the Monte Carlo simulation, we now estimate the R_V for the dust in host galaxies of a sample of 109 observed low redshift ($\lesssim 0.1$) SNe Ia, collected by Wang et al. (2006) and for which they determined the reddening distribution of SNe in their respective host galaxies. We grouped these SNe by host galaxy morphology as per the KINGFISH galaxies, resulting in 7, 21, 34, 7, 17 and 1 galaxies classified as Sa-Sap, Sab-Sbp, Sbc-Scp, Scd-Sdm, S0 and Irregulars respectively.

The color excess E(B-V) = A_V/R_V is measured by assuming an intrinsic brightness and a distance. It depends on A_V, which depends on the dust mass column density, and on R_V, which depends on physical properties of dust. If we now assume that the distribution of dust, i.e. the most probable color excess caused by dust extinction in galaxies can be described with functions given in Table 4.1, for a fixed extinction A_V, i.e. fixed dust amount, varying R_V changes the color excess E(B-V). Thus, we use the least square method to determine a factor at which our functions of most probable color excess (Table 4.1) best fit the Wang et al. (2006) sample. We then estimate the R_V of the sample by dividing 3.1 with the determined factor.

Wang et al. (2006) calculated host galaxy reddening by averaging E(B-V) determined from the (B-V) color curve at late times (cf. Lira, 1995) and E(B-V) determined from (B-V) 12 days after maximum, ΔC_{12}. SNe absolute V magnitudes were then calculated as a function of ΔC_{12}, and plotted against E(B-V) of the host galaxies. The slope is R_V. They derive $R_V = 2.30 \pm 0.11$, and suggest that the remarkably small scatter indicates that the dust properties are similar in z $\lesssim 0.1$ host galaxies.

We use our reddening statistics to estimate the R_V value for the Wang et al. (2006) subsamples of 21 Ia SNe observed in Sab-Sbp galaxies, and 34 SNe in Sbc-Scp. We find

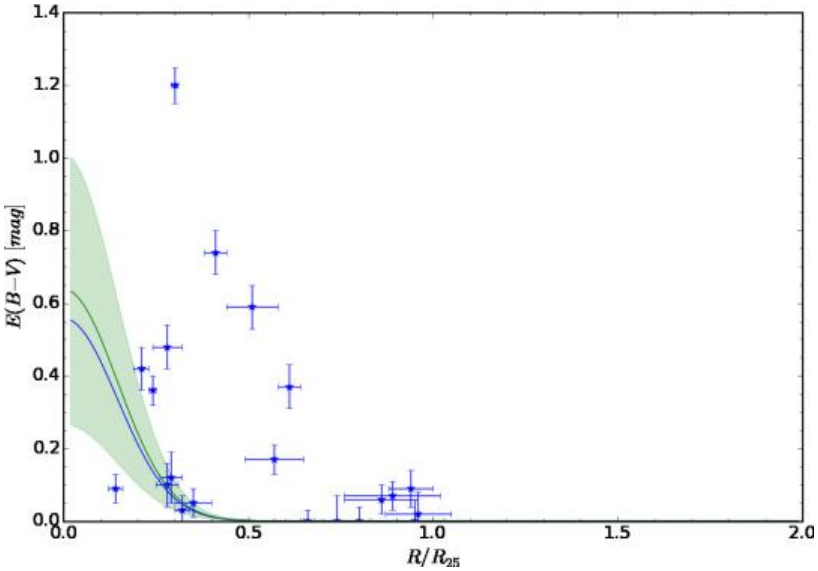

Figure 4.2: Blue crosses show a sample of 21 Ia SNe in Sab-Sbp galaxies. The sample best matches the function of most probable color excess for SNe Ia in Sab-Sbp galaxies (blue line) if multiplied by 1.14 ± 0.67 (green line). The shaded green is the 1-σ uncertainty.

that our function of galactocentric distance for most probable color excess E(B-V) best matches the sample of observed SNe in Sab-Sbp galaxies if multiplied with 1.14 ± 0.67 (Figure 4.2), which corresponds to $R_V = 2.71 \pm 1.58$. In the case of SNe in Sbc-Scp galaxies, we find $R_V = 1.70 \pm 0.38$ (Figure 4.3). Both R_V values are smaller than the common ratio for Milky way dust, which is consistent with the recent earlier studies (see Table 1.1). This method of R_V estimation requires a large sample of observed SNe. The subsample of 7, 7, 17 and 1 observed SNe in Sa-Sap, Scd-Sdm, S0 and Irregulars respectively, is not enough to get a reasonable result.

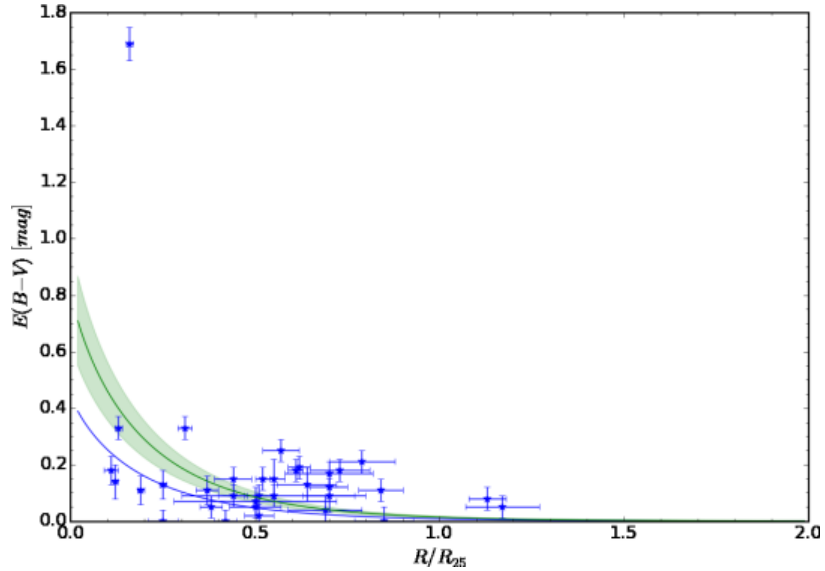

Figure 4.3: Blue crosses show a sample of 34 Ia SNe in Sbc-Scp galaxies from Wang et al. The sample best matches the function of most probable color excess for SNe Ia in Sbc-Scp galaxies (blue line) if multiplied by 1.82 $\pm$ 0.41 (green line). The shaded green is the 1-σ uncertainty.

4.3 Model uncertainty and effect on results

The main uncertainty which can significantly affect the results is the systematic uncertainty of dust masses. Our integrated dust masses are consistent with the masses calculated by Skibba et al. (2011), but there is a discrepancy with dust masses determined by Draine et al. (2007) and Gordon (2008), who use different methods. Gordon (2008) estimated the masses from 70 micron to 160 micron flux ratio, assuming the dust radiates as a black body with emissivity $\propto \lambda^{-2}$, a simple dust model consisting of 0.1 micron silicon grains. Draine et al. (2007) calculated the masses by fitting a multicomponent dust model to the galaxy spectral energy distribution.

For each galaxy in our sample (Table 2.1) we computed dust mass ratios of the Draine, Gordon and Skibba values. The distribution is shown in Figure 4.4. Our dust masses, are in average 2.02 $\pm$ 1.07 and 3.12 $\pm$ 2.24 times lower than the masses derived using Karl Gordon's dust mass maps, and the masses determined by Draine et al. (2007) respectively. The median of the ratios of Gordon's to our, and Draine's to our masses are 1.8, and 2.4 respectively. The discrepancy in the dust mass may be caused by different dust temperature estimates, dust models, but are also correlated with the distance to the galaxies. We used distances given in Skibba et al. (2011) which they took from Kennicutt et al. (2011), while Draine et al. (2007) use distances from Kennicutt et al. (2003). Calculating the dust masses with distances from Kennicutt et al. (2003) give us 2.7 $\pm$ 1.3, and 1.8 $\pm$ 0.7 times lower masses from Draine et al. (2007) and Gordon respectively. The dust mass ratios are summarized in Table 4.2.

The total dust mass is linearly related to A_V and E(B-V), and thus the color excess functions given in Table 4.1. If there would hypothetically be twice as much dust in our model, the color excess would be twice as large, and the estimated R_V ratios would be larger; R_V = 3.40 $\pm$ 0.76 for Sab-Sb, and R_V = 5.42 $\pm$ 3.16 for Sbc-Sc.

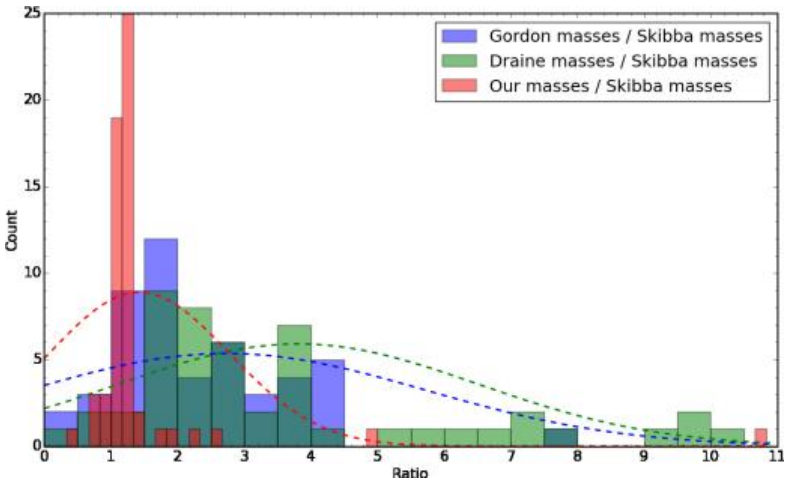

Figure 4.4: Ratios of Gordon, Draine and our dust masses to Skibba dust masses (blue, green and red bars respectively). The blue, green and red lines are gaussian fits of the corresponding histograms. The average dust mass ratios for $Gordon/Skibba$ = 2.73 with σ = 2.98, for $Draine/Skibba$ = 3.81 with σ = 2.70, and for $Our/Skibba$ = 1.42 with σ = 1.34.

Table 4.2: Dust mass ratio comparison

Distances	Skibba et al. (2011)		Kennicutt et al. (2003)	
Ratio	Mean	Median	Mean	Median
Our/Skibba	1.43(1.35)	1.18	1.54(1.38)	1.20
Draine/Skibba	3.81(2.70)	2.73	...	...
Gordon/Skibba	2.73(2.98)	1.97	...	...
Draine/Our	3.12(2.24)	2.35	2.73(1.31)	2.46
Gordon/Our	2.02(1.07)	1.82	1.82(0.72)	1.74

Chapter 5

Summary and conclusions

- We use dust temperature estimations by Skibba et al. (2011) and Herschel 500μm SPIRE maps to create pixel-by-pixel dust mass surface density maps for a sample of 59 KINGFISH galaxies (Kennicutt et al., 2011).
- We compare our model to SN 1989B, SN 2002bo and SN 2006X, three individual Ia SNe which occured in one of the KINGFISH galaxies, and have shown that our model is in good agreement with the observations. We are able explain and reproduce the observed spectra.
- We group the sample into six groups according to the morphology, and run a Monte Carlo simulation to place constrains of color excess as a function of galactocentric distance. We developed a color excess probability model due to dust extinction and have shown the differences between the morphological galaxy classifications. We find that largest reddening probability can be expected in Sab-Sab and Sbc-Sc galaxies, while S0 and Irregulars are very dust poor. We determine the most probable reddening for different galaxy classes as a function of R/R_{25} (Table 4.1). The functions can be used to estimate reddening of type Ia SNe depending on the host galaxy morphology and the galactocentric distance of the observed SNe, or for extinction correction studies for Type Ia supernova rates (e.g. Riello and Patat (2005)).
- We present a new approach for determination of the absorption-to-reddening ratio R_V using statistics of color excess developed in a Monte Carlo simulation. We find for a sample of 21 Ia SNe observed in Sab-Sbp galaxies, and 34 SNe in Sbc-Scp, an R_V of 2.71 $\pm$ 1.58 and R_V=1.70 $\pm$ 0.38 respectively, but the results strongly depend on the certainty of dust masses.

Appendix A

KINGFISH galaxies dust mass surface density maps

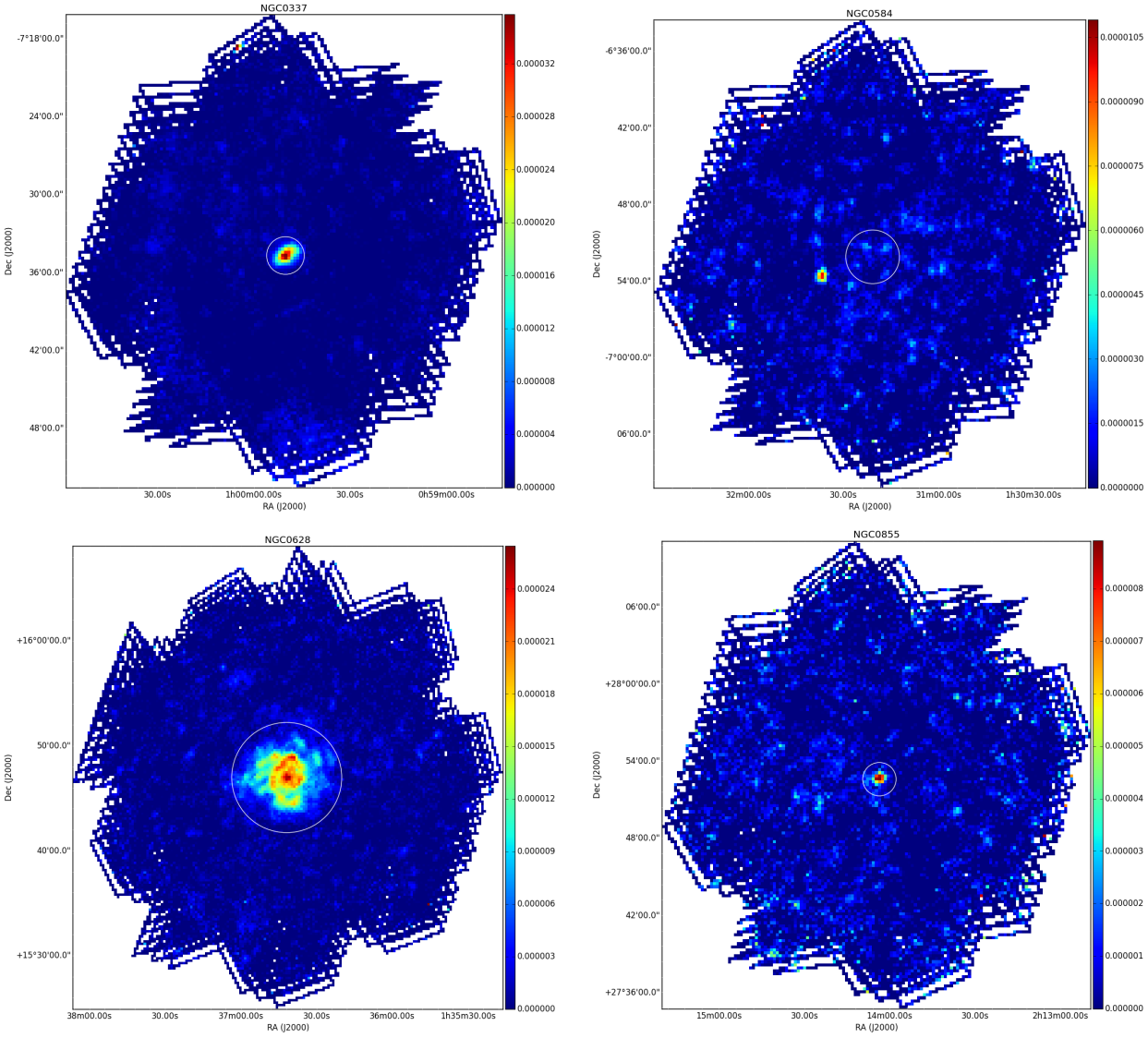

Figure A.1: KINGFISH galaxies dust mass surface density maps. The color indicates the surface density in $g\ cm^{-2}$. The radius of the circle is R_{25}.

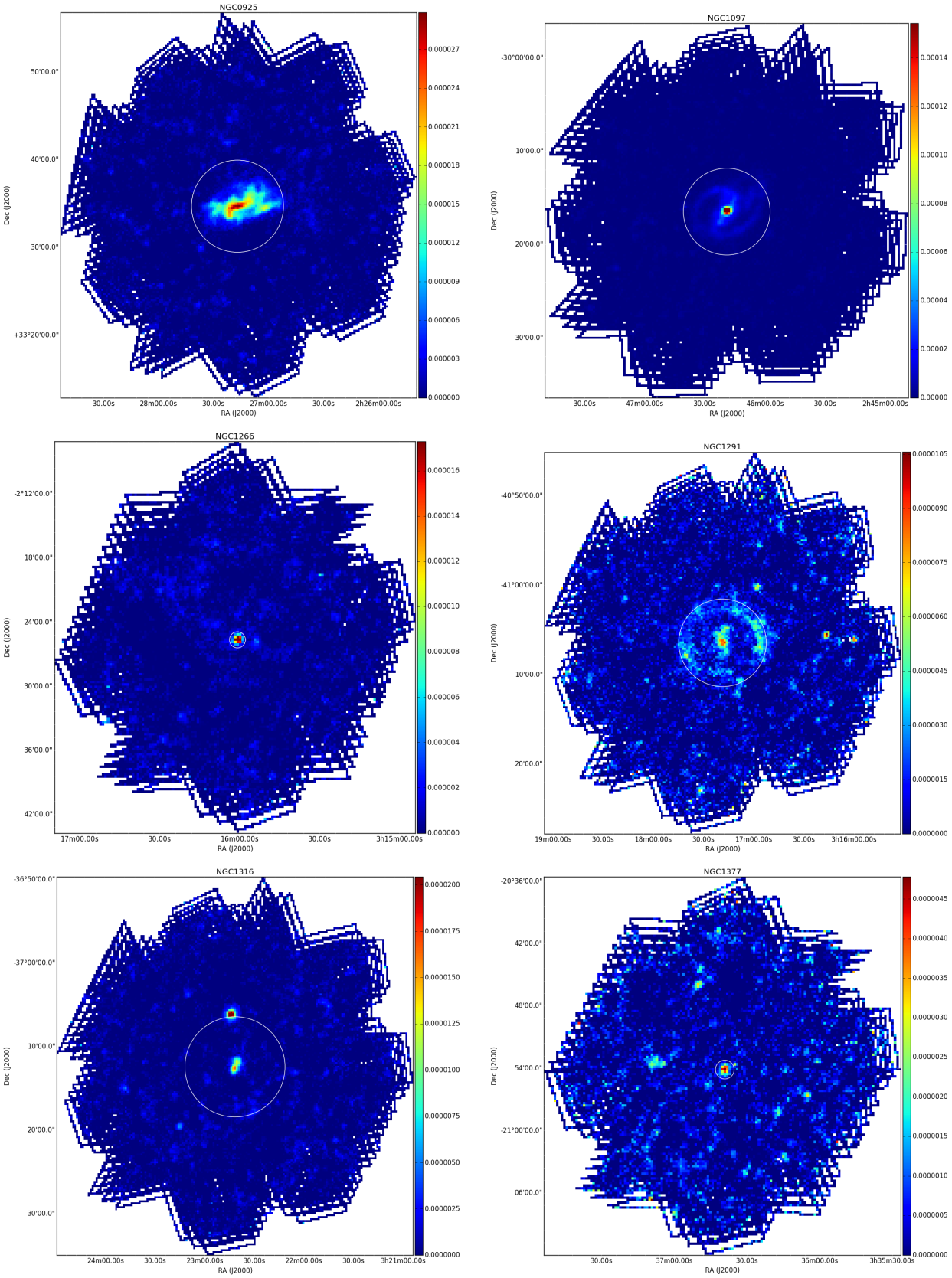

Figure A.1: continuation...

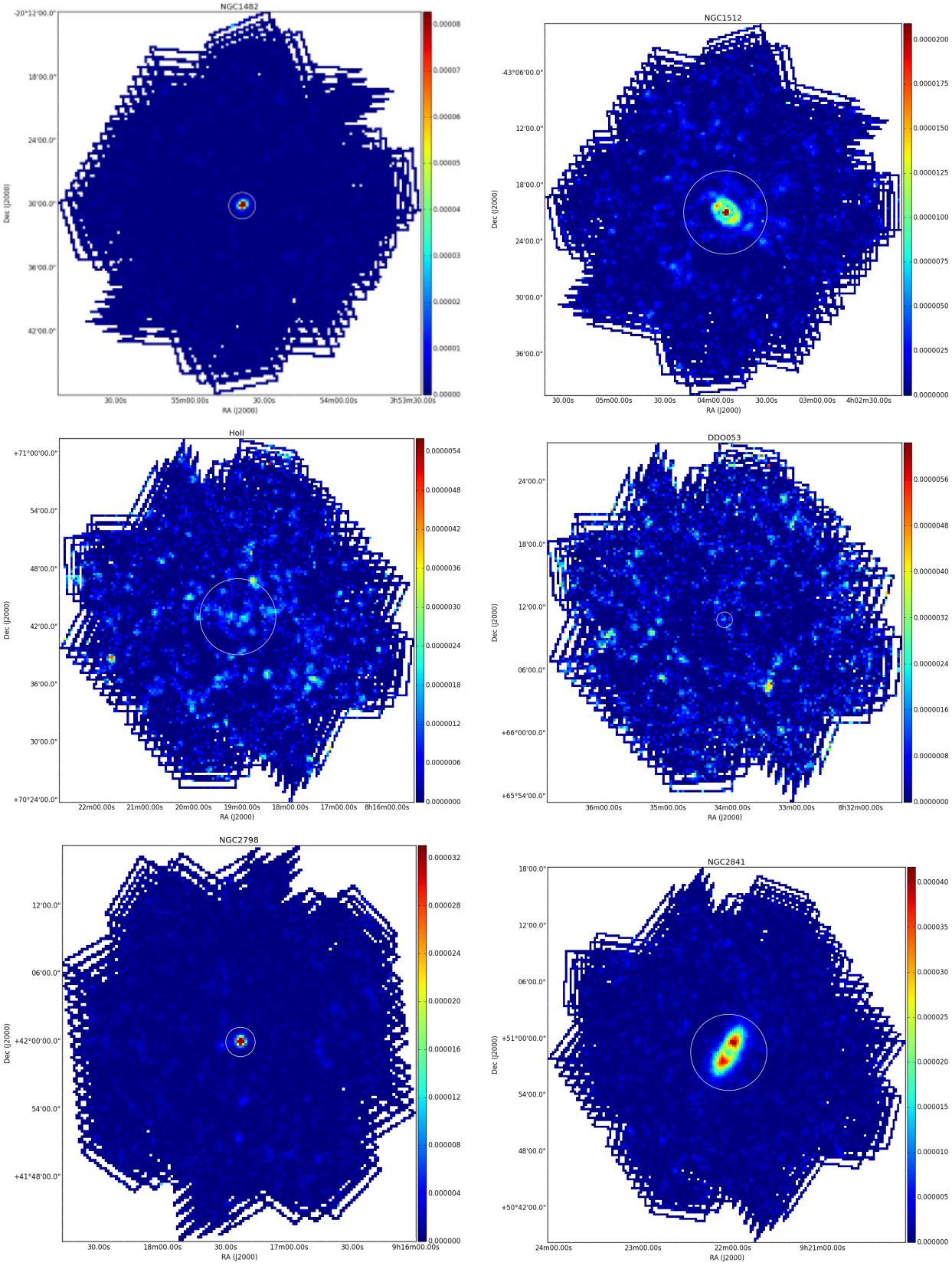

Figure A.1: continuation...

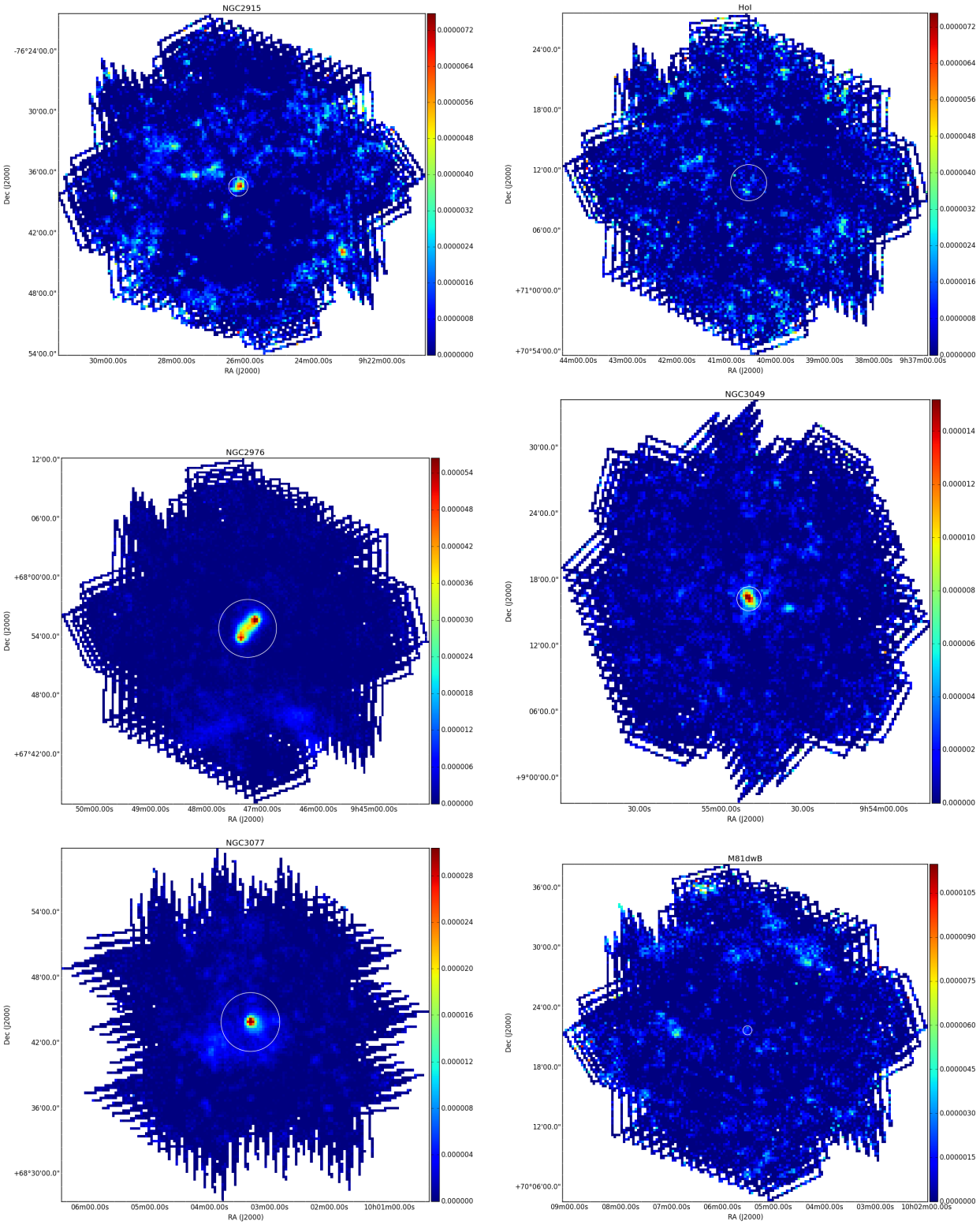

Figure A.1: continuation...

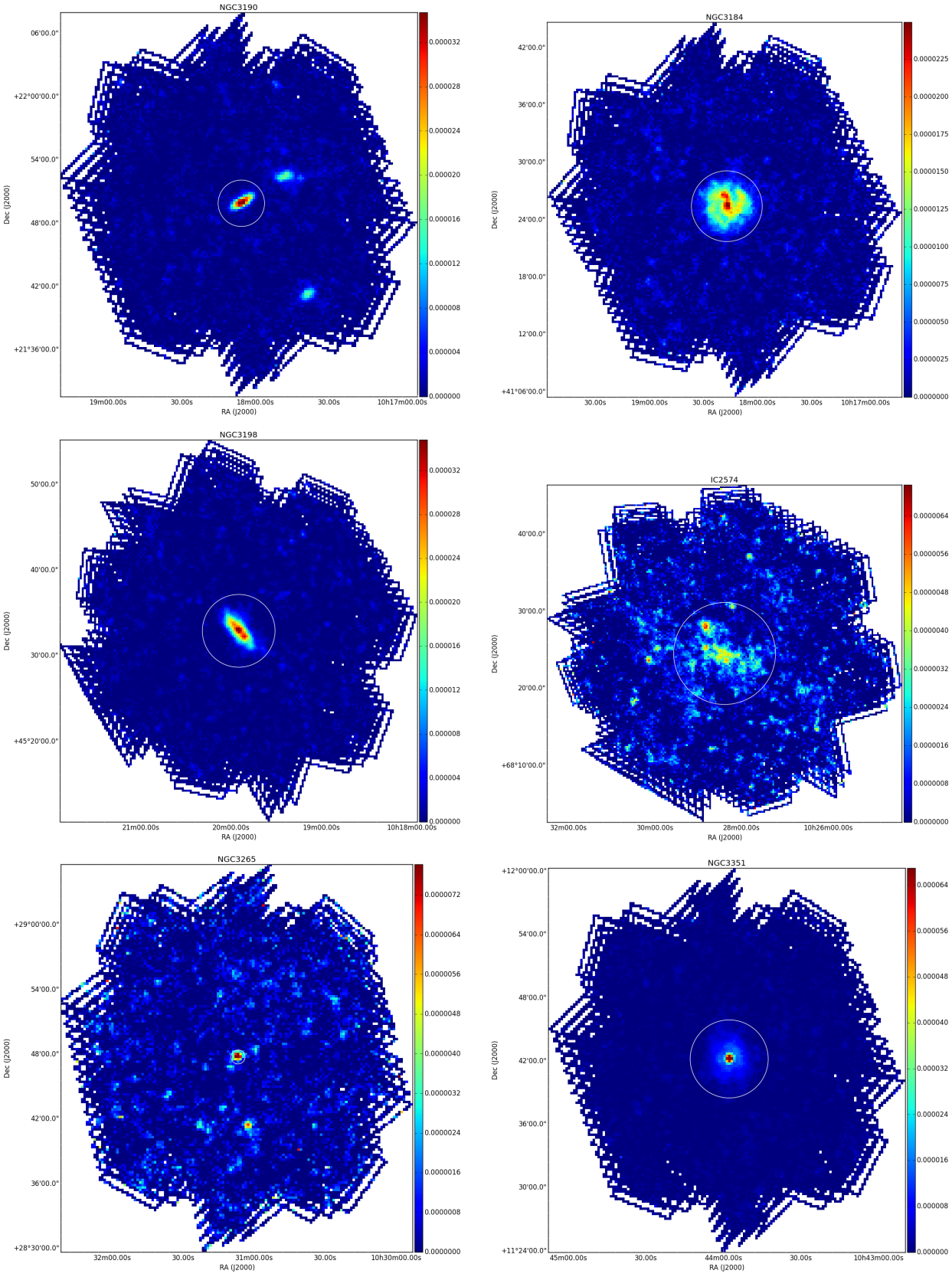

Figure A.1: continuation...

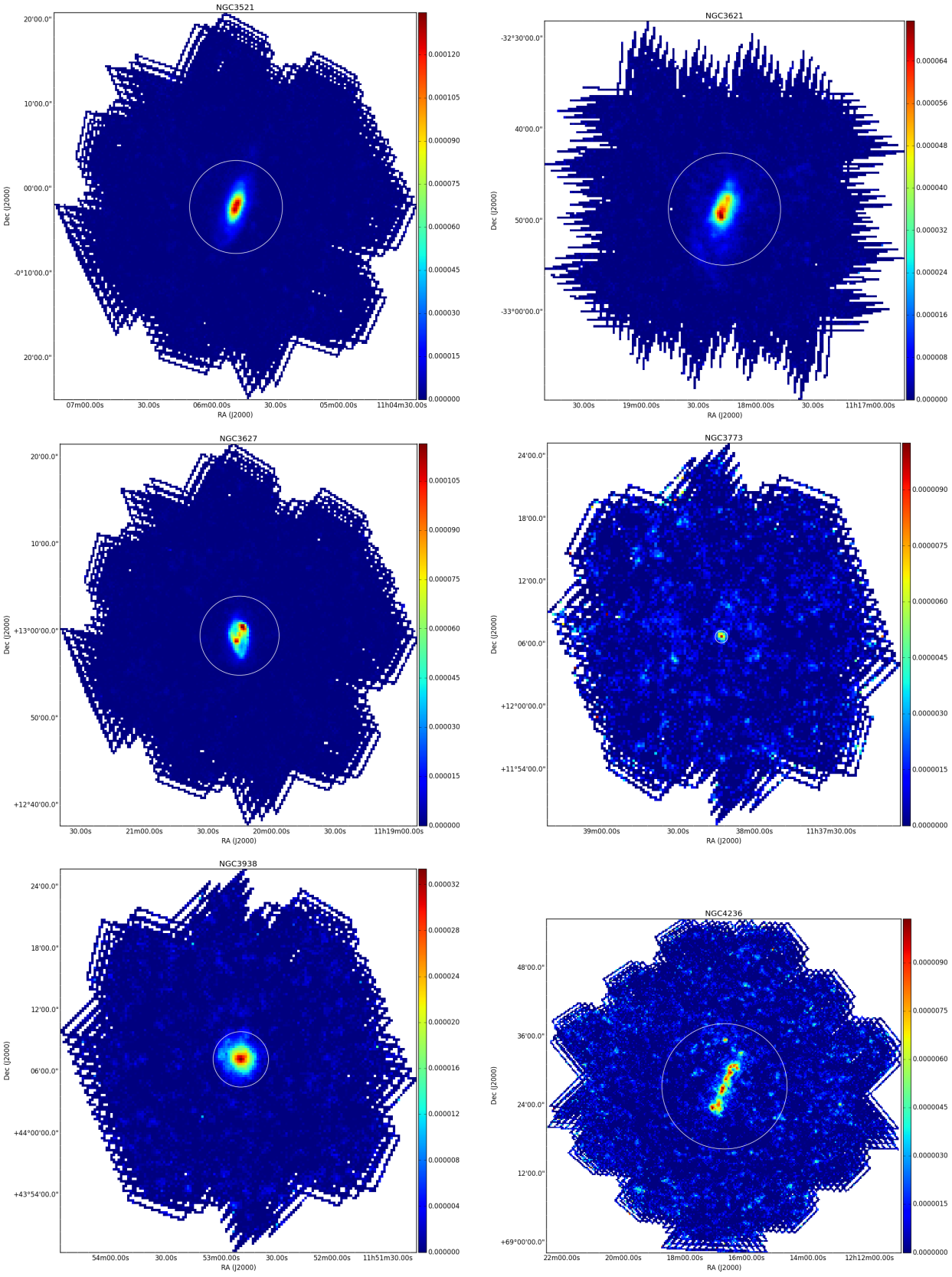

Figure A.1: continuation...

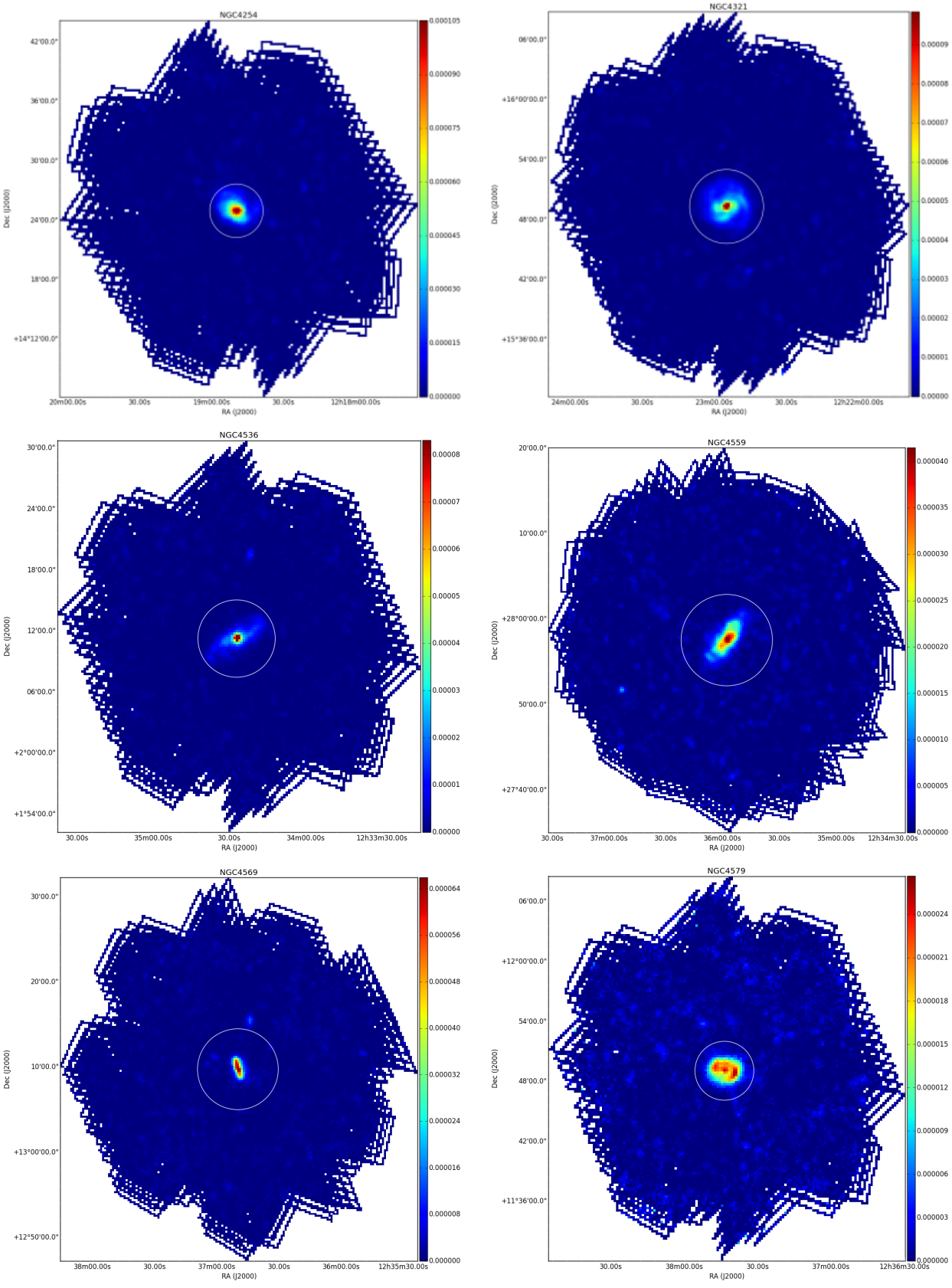

Figure A.1: continuation...

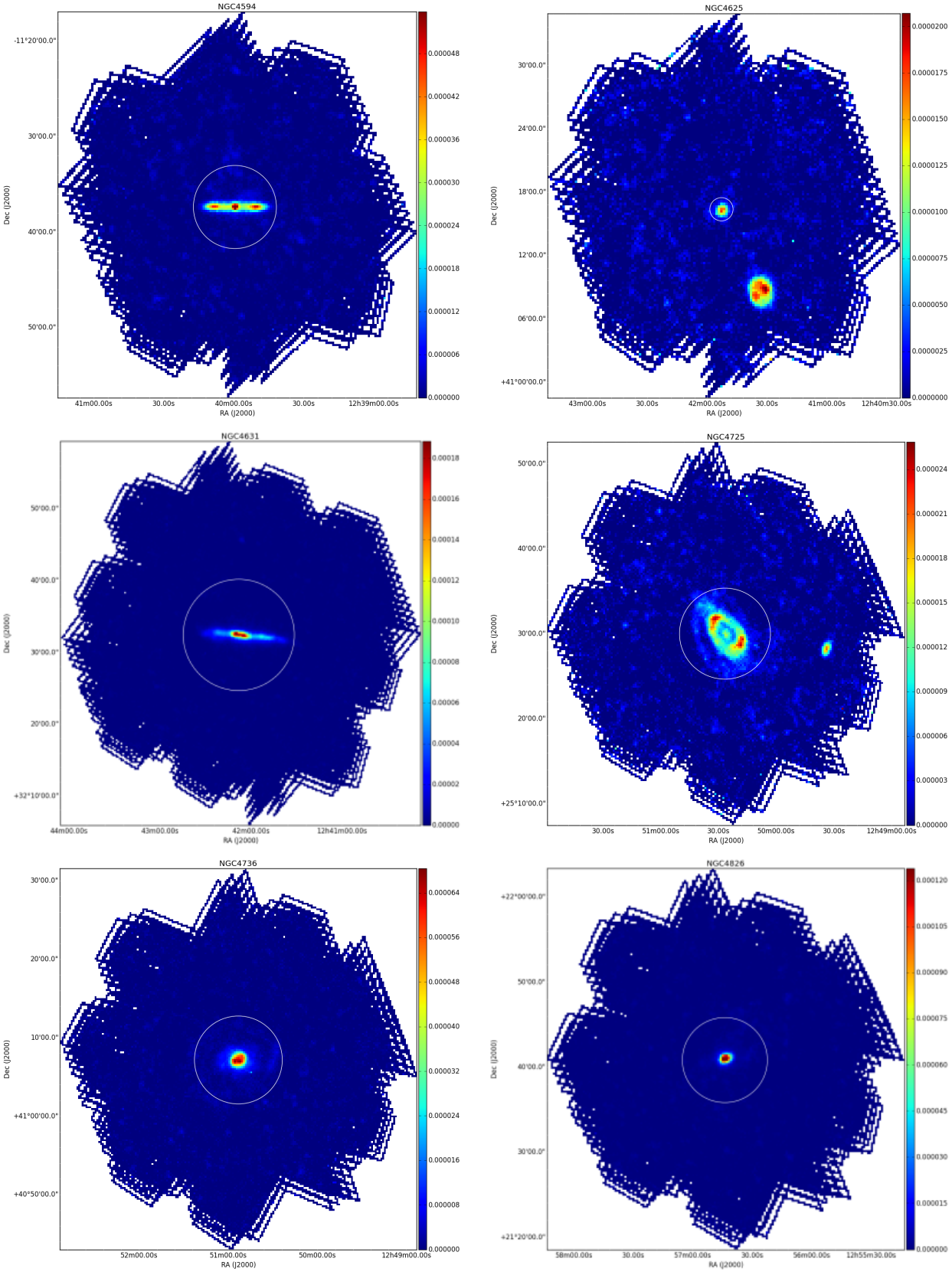

Figure A.1: continuation...

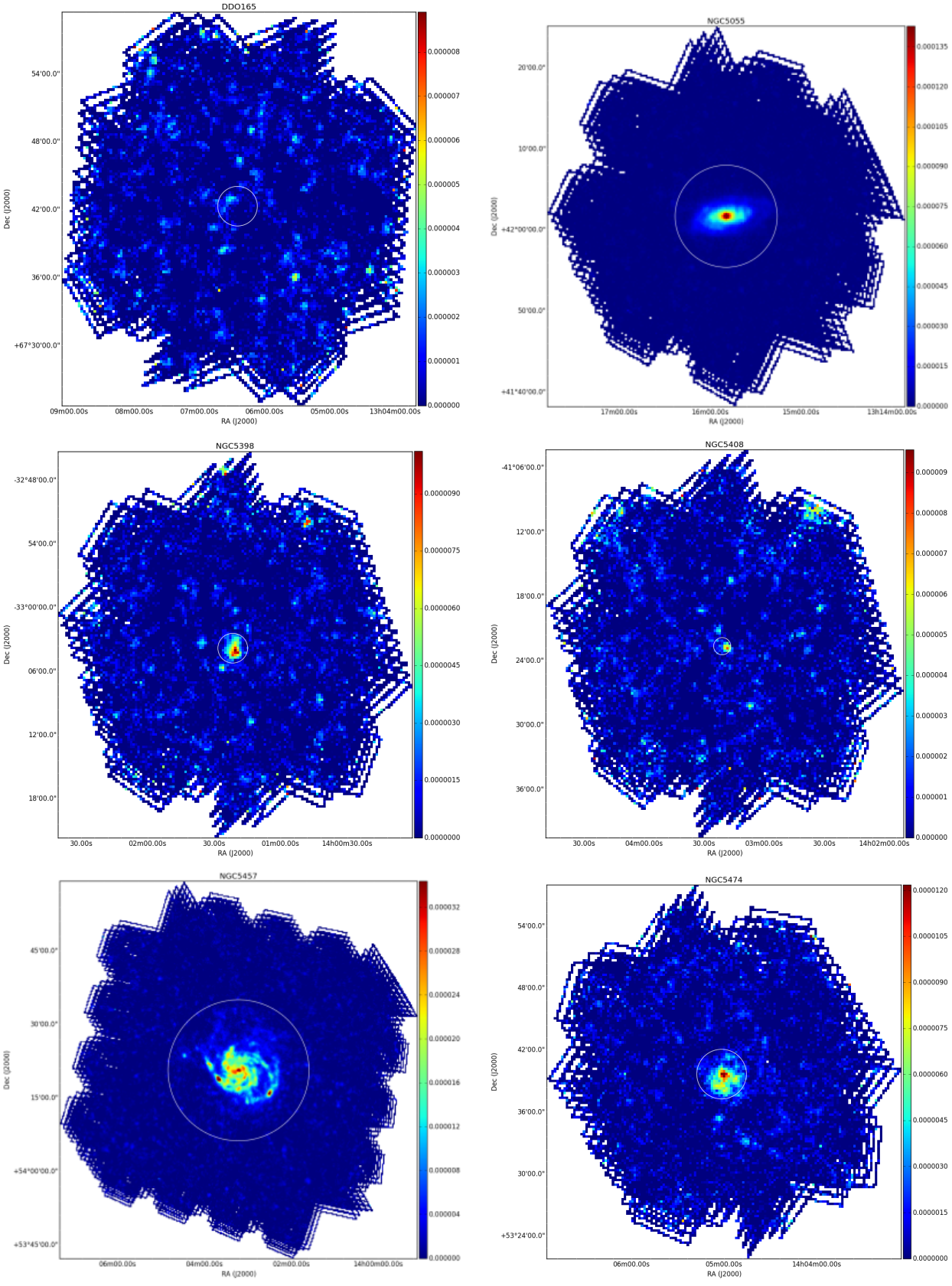

Figure A.1: continuation...

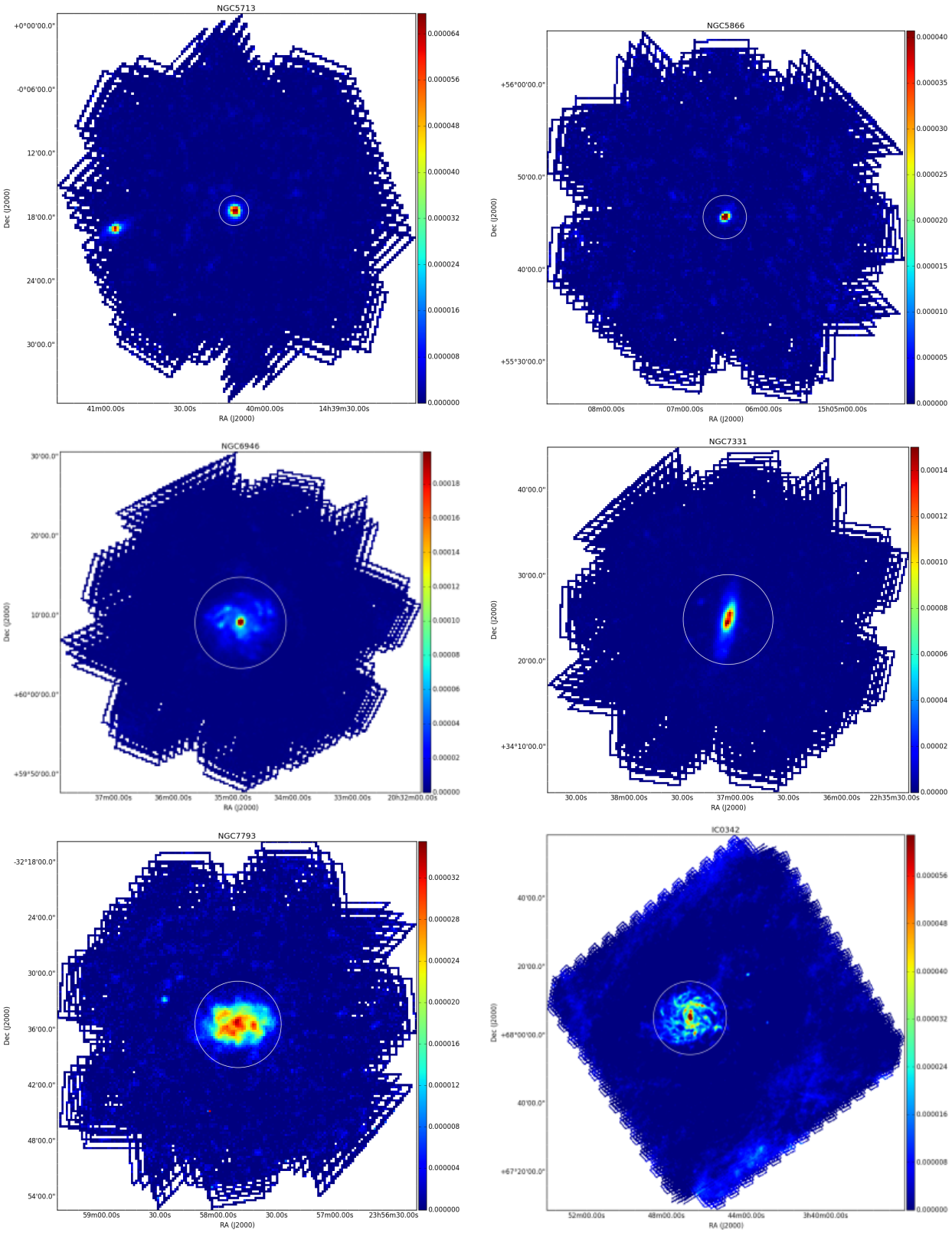

Figure A.1: continuation...

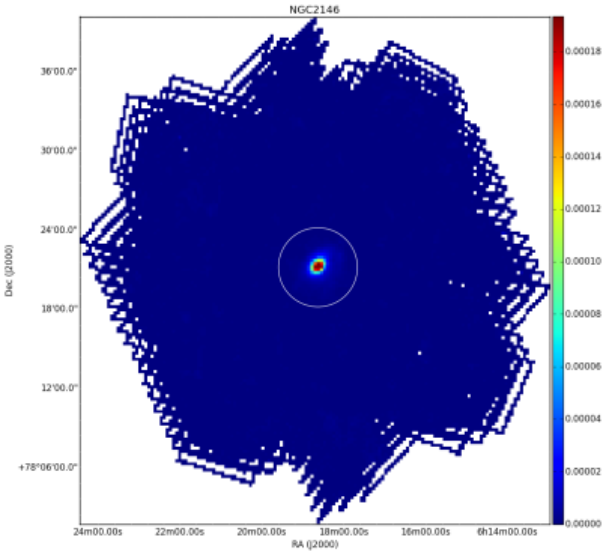

Figure A.1: continuation...

Appendix B

SNe in KINGFISH galaxies

B.1 SN 1989B

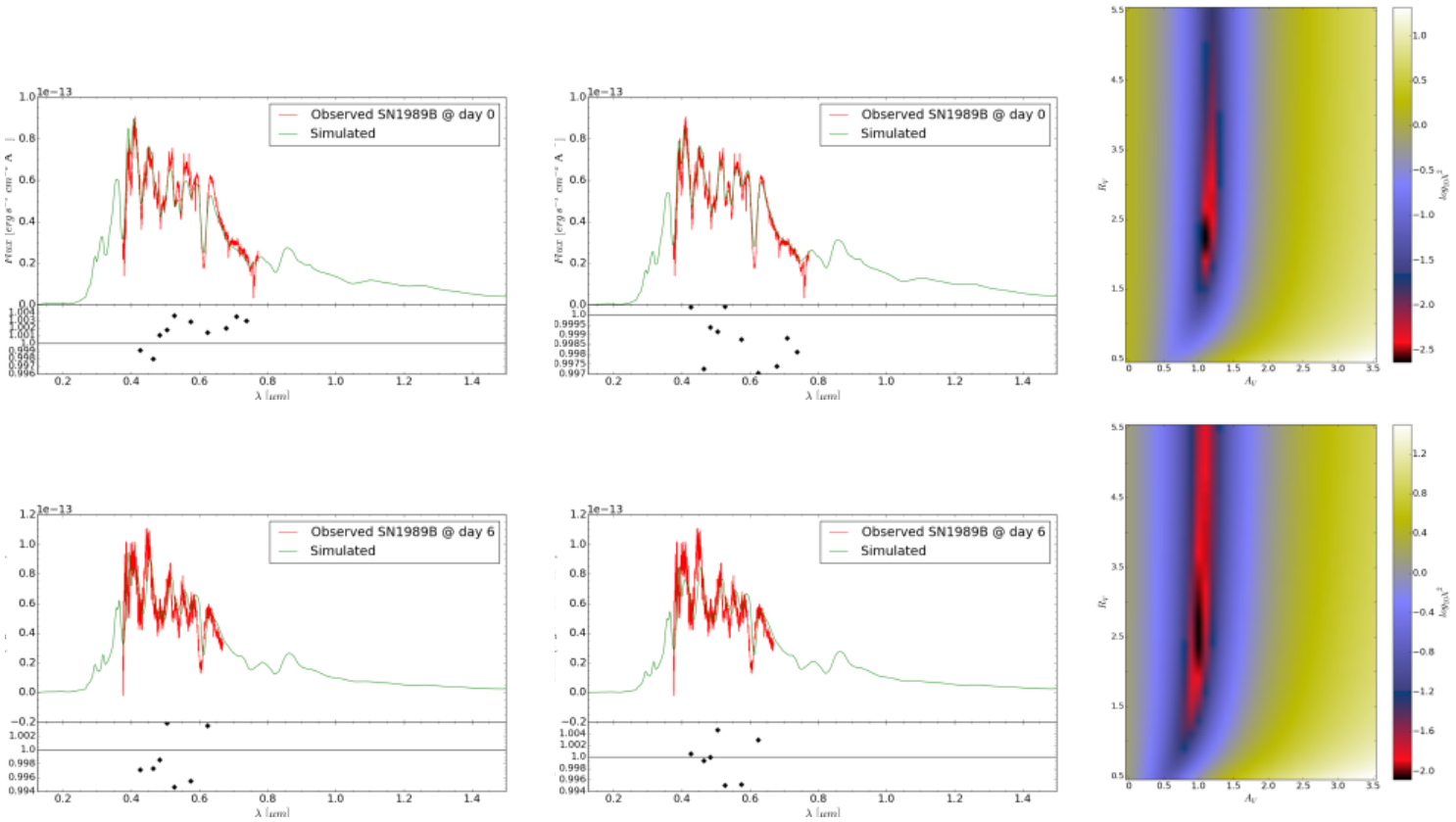

Figure B.1: *Left column:* Comparison between the observed SN 1989B spectra at different epochs and the best fit spectral template, obtained by applying extinction law with R_V = 3.1 and different A_V values. *Middle column:* Comparison between the observed spectra and the best fit template obtained by applying an extinction law with a range of different R_V and A_V values. *Right column:* The distribution of χ^2 values for the matching procedure.

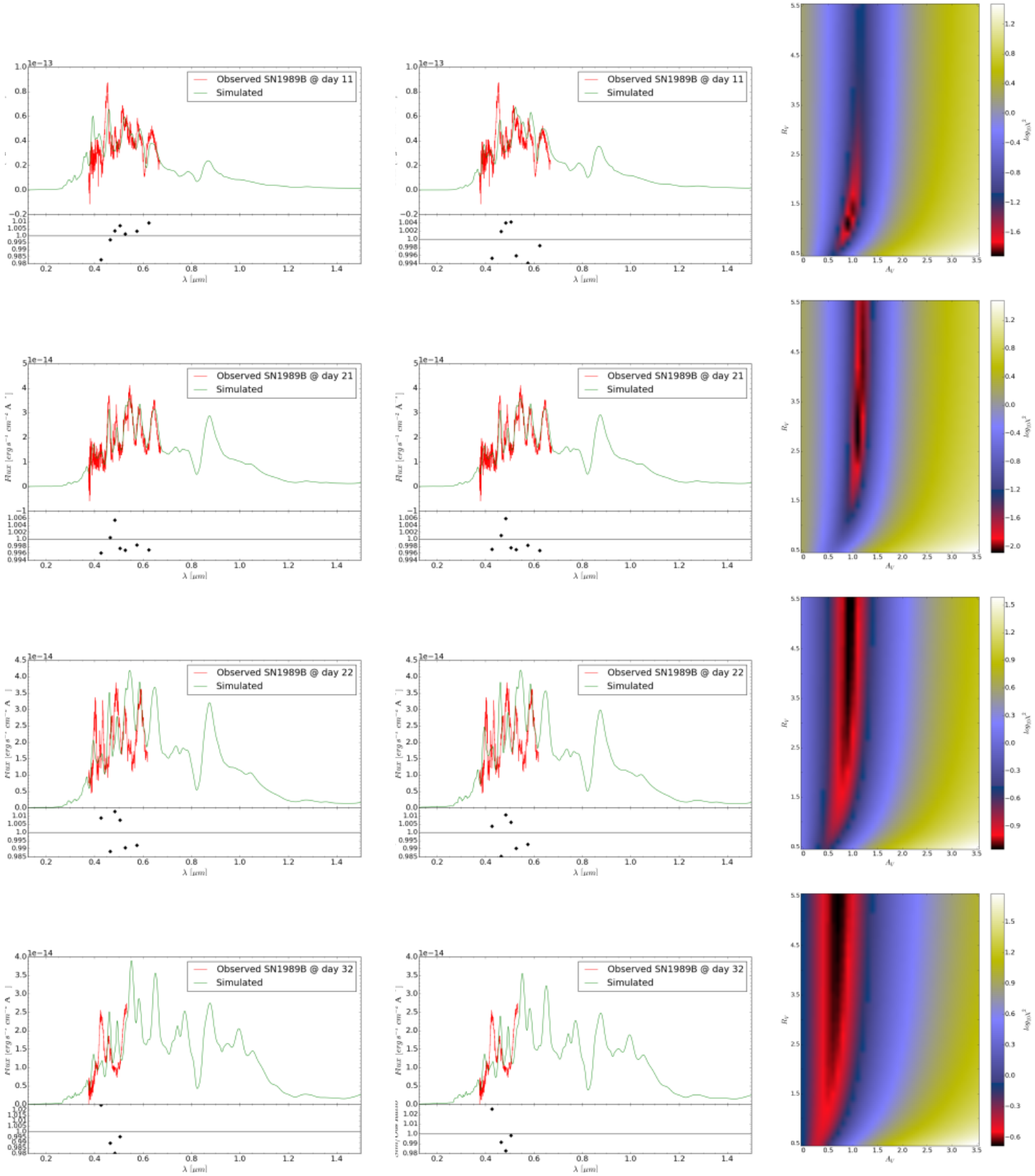

Figure B.1: continuation...

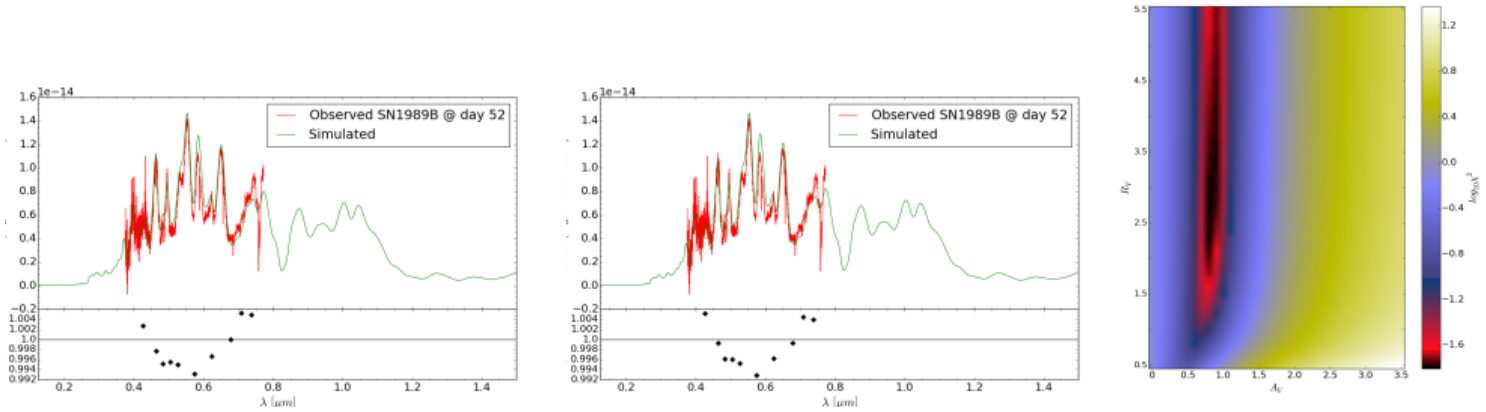

Figure B.1: continuation...

B.2 SN 2002bo

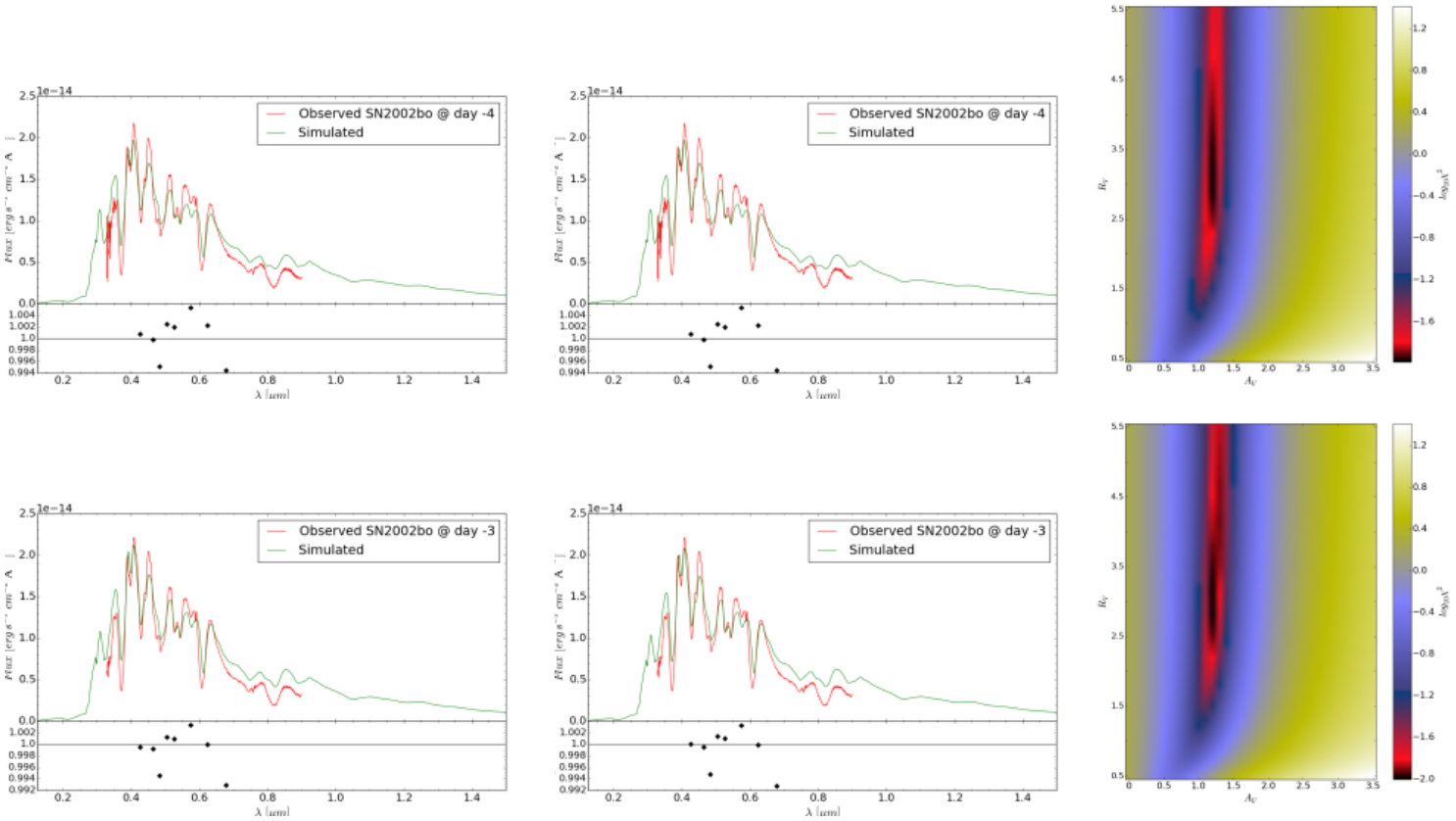

Figure B.2: *Left column:* Comparison between the observed SN 2002bo spectra at different epochs and the best fit spectral template, obtained by applying extinction law with R_V = 3.1 and different A_V values. *Middle column:* Comparison between the observed spectra and the best fit template obtained by applying an extinction law with a range of different R_V and A_V values. *Right column:* The distribution of χ^2 values for the matching procedure.

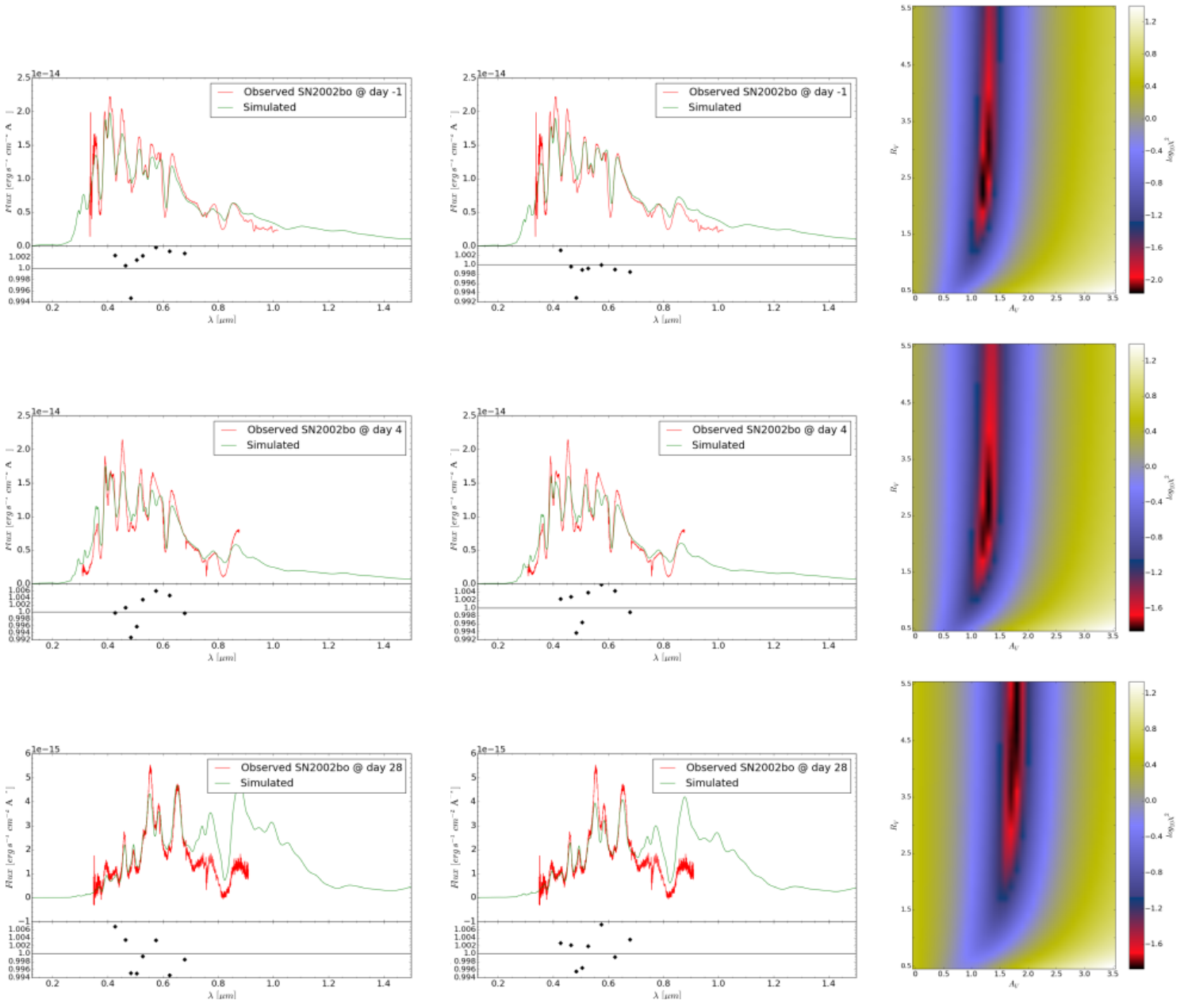

Figure B.1: continuation...

B.3 SN 2006X

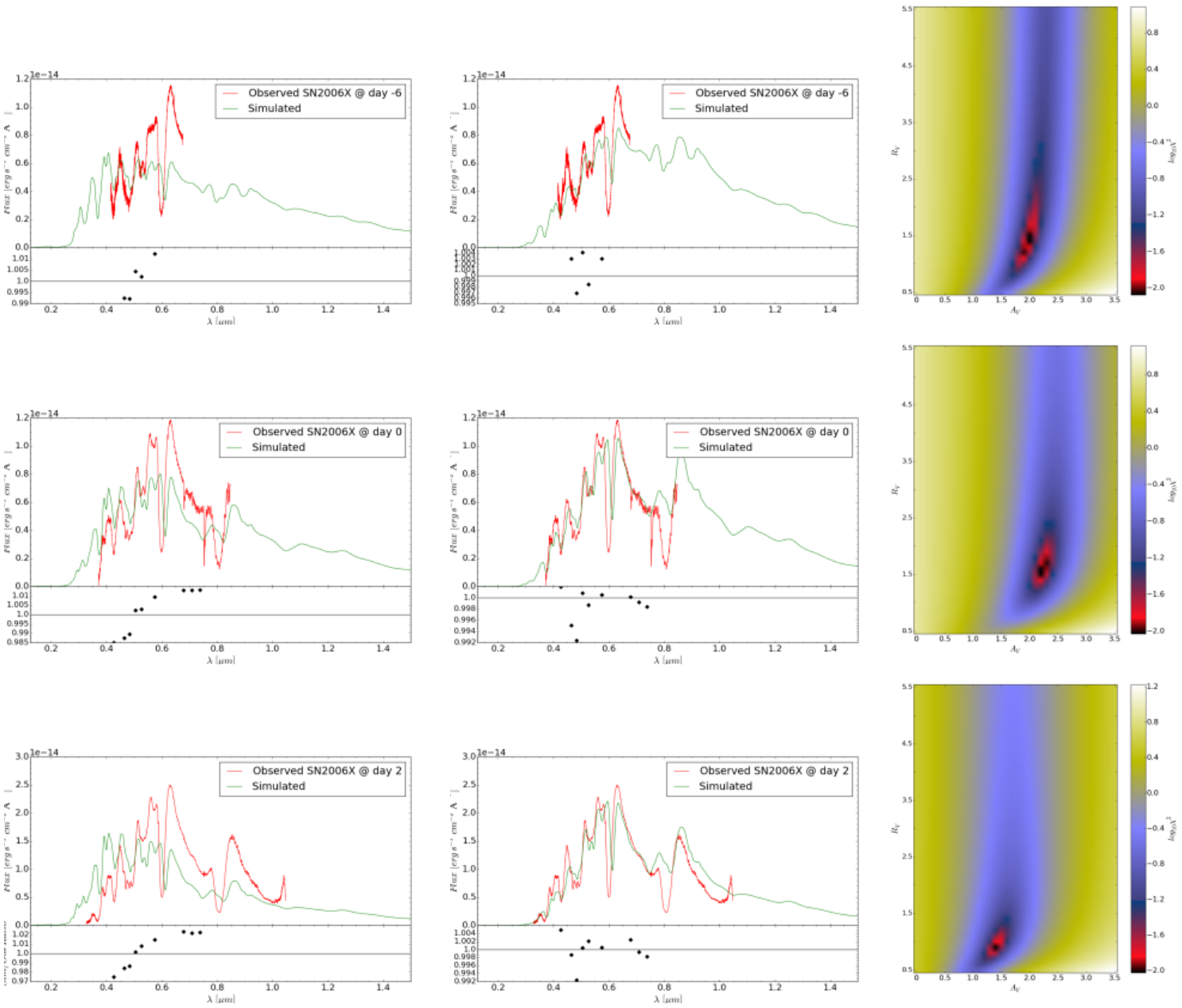

Figure B.2: *Left column:* Comparison between the observed SN 2006X spectra at different epochs and the best fit spectral template, obtained by applying extinction law with R_V = 3.1 and different A_V values. *Middle column:* Comparison between the observed spectra and the best fit template obtained by applying an extinction law with a range of different R_V and A_V values. *Right column:* The distribution of χ^2 values for the matching procedure.

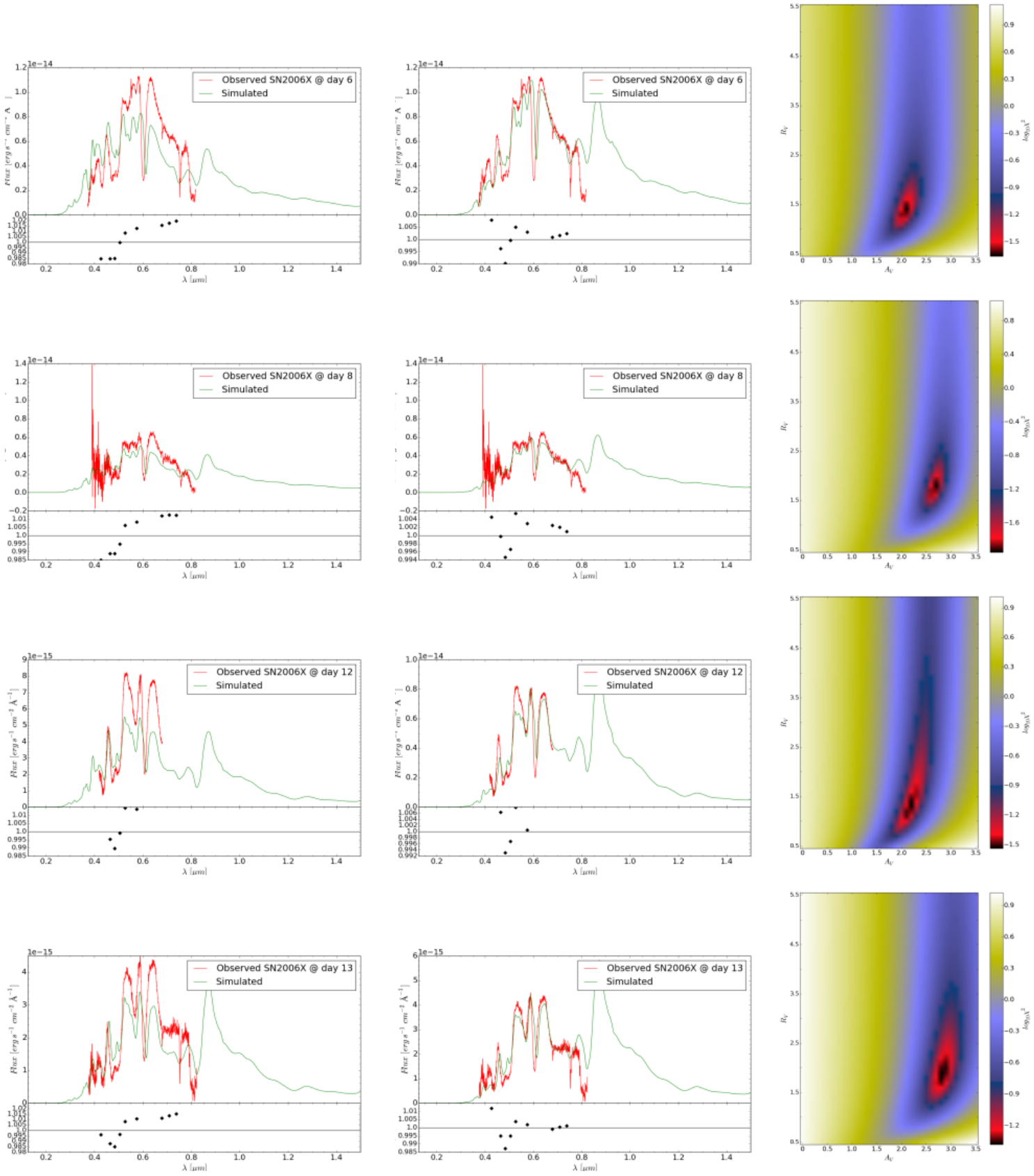

Figure B.1: continuation...

Acknowledgements

I thank to Dr. Susana Deustua for the supervision, support and hosting me at the Space Telescope Science institute in Baltimore, MD during a research internship from March to July 2015.

This work was supported by the STScI Summer Student Program and the STScI Director's Discretionary Research Fund. We thank Eric Hsiao for reading the draft paper and giving comments, Karl Gordon for providing his SINGS galaxies dust mass maps, and Bruce Draine, Andrew Howell, Nick Mostek and Andy Fruchter for helpful discussions and advice.

In Figure 3.3 and 3.8, we use images based on observations made with the NASA/ESA Hubble Space Telescope, and obtained from the Hubble Legacy Archive, which is a collaboration between the Space Telescope Science Institute (STScI/NASA), the Space Telescope European Coordinating Facility (ST-ECF/ESA) and the Canadian Astronomy Data Centre (CADC/NRC/CSA).

In Figure 3.3 we use a SDSS image of NGC 3627. Funding for the SDSS and SDSS-II has been provided by the Alfred P. Sloan Foundation, the Participating Institutions, the National Science Foundation, the U.S. Department of Energy, the National Aeronautics and Space Administration, the Japanese Monbukagakusho, the Max Planck Society, and the Higher Education Funding Council for England. The SDSS Web Site is http://www.sdss.org/.

The SDSS is managed by the Astrophysical Research Consortium for the Participating Institutions. The Participating Institutions are the American Museum of Natural History, Astrophysical Institute Potsdam, University of Basel, University of Cambridge, Case Western Reserve University, University of Chicago, Drexel University, Fermilab, the Institute for Advanced Study, the Japan Participation Group, Johns Hopkins University, the Joint Institute for Nuclear Astrophysics, the Kavli Institute for Particle Astrophysics and Cosmology, the Korean Scientist Group, the Chinese Academy of Sciences (LAMOST), Los Alamos National Laboratory, the Max-Planck-Institute for Astronomy (MPIA), the Max-Planck-Institute for Astrophysics (MPA), New Mexico State University, Ohio State University, University of Pittsburgh, University of Portsmouth, Princeton University, the United States Naval Observatory, and the University of Washington.

Bibliography

G. Altavilla, G. Fiorentino, M. Marconi, I. Musella, E. Cappellaro, R. Barbon, S. Benetti, A. Pastorello, M. Riello, M. Turatto, and L. Zampieri. Cepheid calibration of Type Ia supernovae and the Hubble constant. *MNRAS*, 349:1344–1352, April 2004. doi: 10.1111/j.1365-2966.2004.07616.x.

R. Barbon, S. Benetti, L. Rosino, E. Cappellaro, and M. Turatto. Type IA supernova 1989B in NGC 3627. *A&A*, 237:79–90, October 1990.

S. Benetti, P. Meikle, M. Stehle, G. Altavilla, S. Desidera, G. Folatelli, A. Goobar, S. Mattila, J. Mendez, H. Navasardyan, A. Pastorello, F. Patat, M. Riello, P. Ruiz-Lapuente, D. Tsvetkov, M. Turatto, P. Mazzali, and W. Hillebrandt. Supernova 2002bo: inadequacy of the single parameter description. *MNRAS*, 348:261–278, February 2004. doi: 10.1111/j.1365-2966.2004.07357.x.

M. S. Bessell. UBVRI passbands. *PASP*, 102:1181–1199, October 1990. doi: 10.1086/132749.

D. Branch and G. A. Tammann. Type IA supernovae as standard candles. *ARA&A*, 30: 359–389, 1992. doi: 10.1146/annurev.aa.30.090192.002043.

D. Branch, S. W. Falk, A. K. Uomoto, B. J. Wills, M. L. McCall, and P. Rybski. The type II supernova 1979c in M100 and the distance to the Virgo cluster. *ApJ*, 244:780–804, March 1981. doi: 10.1086/158755.

D. Branch, C. H. Lacy, M. L. McCall, P. G. Sutherland, A. Uomoto, J. C. Wheeler, and B. J. Wills. The Type I supernova 1981b in NGC 4536 - The first 100 days. *ApJ*, 270: 123–125, July 1983. doi: 10.1086/161103.

R. J. Buta, K. Sheth, M. Regan, J. L. Hinz, A. Gil de Paz, K. Menéndez-Delmestre, J.-C. Munoz-Mateos, M. Seibert, E. Laurikainen, H. Salo, D. A. Gadotti, E. Athanassoula, A. Bosma, J. H. Knapen, L. C. Ho, B. F. Madore, D. M. Elmegreen, K. L. Masters, S. Comerón, M. Aravena, and T. Kim. Mid-infrared Galaxy Morphology from the Spitzer Survey of Stellar Structure in Galaxies (S^4G): The Imprint of the De Vaucouleurs Revised Hubble-Sandage Classification System at 3.6 μm. *ApJS*, 190:147–165, September 2010. doi: 10.1088/0067-0049/190/1/147.

E. Cappellaro and M. Turatto. Supernova Types and Rates. In D. Vanbeveren, editor, *The Influence of Binaries on Stellar Population Studies*, volume 264 of *Astrophysics and Space Science Library*, page 199, 2001.

J. A. Cardelli, G. C. Clayton, and J. S. Mathis. The relationship between infrared, optical, and ultraviolet extinction. *ApJ*, 345:245–256, October 1989. doi: 10.1086/167900.

D. Casebeer, D. Branch, M. Blaylock, J. Millard, E. Baron, D. Richardson, and C. Ancheta. Lick Observatory Photographic Supernova Spectra. *PASP*, 112:1433–1438, November 2000. doi: 10.1086/317699.

A. Conley, R. G. Carlberg, J. Guy, D. A. Howell, S. Jha, A. G. Riess, and M. Sullivan. Is There Evidence for a Hubble Bubble? The Nature of Type Ia Supernova Colors and Dust in External Galaxies. *ApJ*, 664:L13–L16, July 2007. doi: 10.1086/520625.

G. de Vaucouleurs, A. de Vaucouleurs, H. G. Corwin, Jr., R. J. Buta, G. Paturel, and P. Fouqué. *Third Reference Catalogue of Bright Galaxies. Volume I: Explanations and references. Volume II: Data for galaxies between 0^h and 12^h. Volume III: Data for galaxies between 12^h and 24^h.* 1991.

B. T. Draine. Interstellar Dust Grains. *ARA&A*, 41:241–289, 2003a. doi: 10.1146/annurev.astro.41.011802.094840.

B. T. Draine. Scattering by Interstellar Dust Grains. II. X-Rays. *ApJ*, 598:1026–1037, December 2003b. doi: 10.1086/379123.

B. T. Draine, D. A. Dale, G. Bendo, K. D. Gordon, J. D. T. Smith, L. Armus, C. W. Engelbracht, G. Helou, R. C. Kennicutt, Jr., A. Li, H. Roussel, F. Walter, D. Calzetti, J. Moustakas, E. J. Murphy, G. H. Rieke, C. Bot, D. J. Hollenbach, K. Sheth, and H. I. Teplitz. Dust Masses, PAH Abundances, and Starlight Intensities in the SINGS Galaxy Sample. *ApJ*, 663:866–894, July 2007. doi: 10.1086/518306.

G. Folatelli, M. M. Phillips, C. R. Burns, C. Contreras, M. Hamuy, W. L. Freedman, S. E. Persson, M. Stritzinger, N. B. Suntzeff, K. Krisciunas, L. Boldt, S. González, W. Krzeminski, N. Morrell, M. Roth, F. Salgado, B. F. Madore, D. Murphy, P. Wyatt, W. Li, A. V. Filippenko, and N. Miller. The Carnegie Supernova Project: Analysis of the First Sample of Low-Redshift Type-Ia Supernovae. *AJ*, 139:120–144, January 2010. doi: 10.1088/0004-6256/139/1/120.

A. Goobar. Low R_V from Circumstellar Dust around Supernovae. *ApJ*, 686:L103–L106, October 2008. doi: 10.1086/593060.

K. D. Gordon, F. Galliano, S. Hony, J.-P. Bernard, A. Bolatto, C. Bot, C. Engelbracht, A. Hughes, F. P. Israel, F. Kemper, S. Kim, A. Li, S. C. Madden, M. Matsuura, M. Meixner, K. Misselt, K. Okumura, P. Panuzzo, M. Rubio, W. T. Reach, J. Roman-Duval, M. Sauvage, R. Skibba, and A. G. G. M. Tielens. Determining dust temperatures and masses in the Herschel era: The importance of observations longward of 200 micron. *A&A*, 518:L89, July 2010. doi: 10.1051/0004-6361/201014541.

Karl Gordon. personal communication, 2008.

E. Y. Hsiao, A. Conley, D. A. Howell, M. Sullivan, C. J. Pritchet, R. G. Carlberg, P. E. Nugent, and M. M. Phillips. K-Corrections and Spectral Templates of Type Ia Supernovae. *ApJ*, 663:1187–1200, July 2007. doi: 10.1086/518232.

R. C. Kennicutt, D. Calzetti, G. Aniano, P. Appleton, L. Armus, P. Beirão, A. D. Bolatto, B. Brandl, A. Crocker, K. Croxall, D. A. Dale, J. D. Meyer, B. T. Draine, C. W. Engelbracht, M. Galametz, K. D. Gordon, B. Groves, C.-N. Hao, G. Helou, J. Hinz, L. K. Hunt, B. Johnson, J. Koda, O. Krause, A. K. Leroy, Y. Li, S. Meidt, E. Montiel, E. J. Murphy, N. Rahman, H.-W. Rix, H. Roussel, K. Sandstrom, M. Sauvage, E. Schinnerer, R. Skibba, J. D. T. Smith, S. Srinivasan, L. Vigroux, F. Walter, C. D. Wilson, M. Wolfire,

and S. Zibetti. KINGFISH – Key Insights on Nearby Galaxies: A Far-Infrared Survey with Herschel: Survey Description and Image Atlas. *PASP*, 123:1347–1369, December 2011. doi: 10.1086/663818.

R. C. Kennicutt, Jr., L. Armus, G. Bendo, D. Calzetti, D. A. Dale, B. T. Draine, C. W. Engelbracht, K. D. Gordon, A. D. Grauer, G. Helou, D. J. Hollenbach, T. H. Jarrett, L. J. Kewley, C. Leitherer, A. Li, S. Malhotra, M. W. Regan, G. H. Rieke, M. J. Rieke, H. Roussel, J.-D. T. Smith, M. D. Thornley, and F. Walter. SINGS: The SIRTF Nearby Galaxies Survey. *PASP*, 115:928–952, August 2003. doi: 10.1086/376941.

R. Kessler, A. C. Becker, D. Cinabro, J. Vanderplas, J. A. Frieman, J. Marriner, T. M. Davis, B. Dilday, J. Holtzman, S. W. Jha, H. Lampeitl, M. Sako, M. Smith, C. Zheng, R. C. Nichol, B. Bassett, R. Bender, D. L. Depoy, M. Doi, E. Elson, A. V. Filippenko, R. J. Foley, P. M. Garnavich, U. Hopp, Y. Ihara, W. Ketzeback, W. Kollatschny, K. Konishi, J. L. Marshall, R. J. McMillan, G. Miknaitis, T. Morokuma, E. Mörtsell, K. Pan, J. L. Prieto, M. W. Richmond, A. G. Riess, R. Romani, D. P. Schneider, J. Sollerman, N. Takanashi, K. Tokita, K. van der Heyden, J. C. Wheeler, N. Yasuda, and D. York. First-Year Sloan Digital Sky Survey-II Supernova Results: Hubble Diagram and Cosmological Parameters. *ApJS*, 185:32–84, November 2009. doi: 10.1088/0067-0049/185/1/32.

H. Lampeitl, M. Smith, R. C. Nichol, B. Bassett, D. Cinabro, B. Dilday, R. J. Foley, J. A. Frieman, P. M. Garnavich, A. Goobar, M. Im, S. W. Jha, J. Marriner, R. Miquel, J. Nordin, L. Östman, A. G. Riess, M. Sako, D. P. Schneider, J. Sollerman, and M. Stritzinger. The Effect of Host Galaxies on Type Ia Supernovae in the SDSS-II Supernova Survey. *ApJ*, 722:566–576, October 2010. doi: 10.1088/0004-637X/722/1/566.

B. Leibundgut. Type Ia Supernovae. *A&A Rev.*, 10:179–209, 2000. doi: 10.1007/s001590000009.

P Lira. Master thesis. Master's thesis, University of Chile, Chile, 1995.

K. S. Mandel, G. Narayan, and R. P. Kirshner. Type Ia Supernova Light Curve Inference: Hierarchical Models in the Optical and Near-infrared. *ApJ*, 731:120, April 2011. doi: 10.1088/0004-637X/731/2/120.

D. L. Miller and D. Branch. Supernova absolute-magnitude distributions. *AJ*, 100:530–539, August 1990. doi: 10.1086/115534.

S. Nobili and A. Goobar. The colour-lightcurve shape relation of type Ia supernovae and the reddening law. *A&A*, 487:19–31, August 2008. doi: 10.1051/0004-6361:20079292.

P. Nugent, A. Kim, and S. Perlmutter. K-Corrections and Extinction Corrections for Type Ia Supernovae. *PASP*, 114:803–819, August 2002. doi: 10.1086/341707.

F. Patat, D. Baade, P. Höflich, J. R. Maund, L. Wang, and J. C. Wheeler. VLT spectropolarimetry of the fast expanding type Ia SN 2006X. *A&A*, 508:229–246, December 2009. doi: 10.1051/0004-6361/200810651.

S. Perlmutter, G. Aldering, G. Goldhaber, R. A. Knop, P. Nugent, P. G. Castro, S. Deustua, S. Fabbro, A. Goobar, D. E. Groom, I. M. Hook, A. G. Kim, M. Y. Kim, J. C. Lee, N. J. Nunes, R. Pain, C. R. Pennypacker, R. Quimby, C. Lidman, R. S. Ellis, M. Irwin, R. G. McMahon, P. Ruiz-Lapuente, N. Walton, B. Schaefer, B. J. Boyle, A. V. Filippenko, T. Matheson, A. S. Fruchter, N. Panagia, H. J. M. Newberg, W. J. Couch, and T. S. C.

Project. Measurements of Ω and Λ from 42 High-Redshift Supernovae. *ApJ*, 517: 565–586, June 1999. doi: 10.1086/307221.

M. M. Phillips. The absolute magnitudes of Type IA supernovae. *ApJ*, 413:L105–L108, August 1993. doi: 10.1086/186970.

M. M. Phillips, P. Lira, N. B. Suntzeff, R. A. Schommer, M. Hamuy, and J. Maza. The Reddening-Free Decline Rate Versus Luminosity Relationship for Type IA Supernovae. *AJ*, 118:1766–1776, October 1999. doi: 10.1086/301032.

B. Reindl, G. A. Tammann, A. Sandage, and A. Saha. Reddening, Absorption, and Decline Rate Corrections for a Complete Sample of Type Ia Supernovae Leading to a Fully Corrected Hubble Diagram to v 30,000 km s^{-1}. *ApJ*, 624:532–554, May 2005. doi: 10.1086/429218.

M. Riello and F. Patat. Extinction correction for Type Ia supernova rates - I. The model. *MNRAS*, 362:671–680, September 2005. doi: 10.1111/j.1365-2966.2005.09348.x.

A. G. Riess, W. H. Press, and R. P. Kirshner. Is the Dust Obscuring Supernovae in Distant Galaxies the Same as Dust in the Milky Way? *ApJ*, 473:588, December 1996. doi: 10.1086/178174.

A. G. Riess, A. V. Filippenko, P. Challis, A. Clocchiatti, A. Diercks, P. M. Garnavich, R. L. Gilliland, C. J. Hogan, S. Jha, R. P. Kirshner, B. Leibundgut, M. M. Phillips, D. Reiss, B. P. Schmidt, R. A. Schommer, R. C. Smith, J. Spyromilio, C. Stubbs, N. B. Suntzeff, and J. Tonry. Observational Evidence from Supernovae for an Accelerating Universe and a Cosmological Constant. *AJ*, 116:1009–1038, September 1998. doi: 10.1086/300499.

A. G. Riess, A. V. Filippenko, W. Li, R. R. Treffers, B. P. Schmidt, Y. Qiu, J. Hu, M. Armstrong, C. Faranda, E. Thouvenot, and C. Buil. The Rise Time of Nearby Type IA Supernovae. *AJ*, 118:2675–2688, December 1999. doi: 10.1086/301143.

A. G. Riess, L.-G. Strolger, J. Tonry, S. Casertano, H. C. Ferguson, B. Mobasher, P. Challis, A. V. Filippenko, S. Jha, W. Li, R. Chornock, R. P. Kirshner, B. Leibundgut, M. Dickinson, M. Livio, M. Giavalisco, C. C. Steidel, T. Benítez, and Z. Tsvetanov. Type Ia Supernova Discoveries at z 1 from the Hubble Space Telescope: Evidence for Past Deceleration and Constraints on Dark Energy Evolution. *ApJ*, 607:665–687, June 2004. doi: 10.1086/383612.

A. Saha, A. Sandage, G. A. Tammann, L. Labhardt, F. D. Macchetto, and N. Panagia. Cepheid Calibration of the Peak Brightness of Type IA Supernovae. IX. SN 1989B in NGC 3627. *ApJ*, 522:802–838, September 1999. doi: 10.1086/307693.

D. J. Schlegel, D. P. Finkbeiner, and M. Davis. Maps of Dust Infrared Emission for Use in Estimation of Reddening and Cosmic Microwave Background Radiation Foregrounds. *ApJ*, 500:525, June 1998. doi: 10.1086/305772.

P. Schneider. *Extragalactic Astronomy and Cosmology*. 2006.

R. A. Skibba, C. W. Engelbracht, D. Dale, J. Hinz, S. Zibetti, A. Crocker, B. Groves, L. Hunt, B. D. Johnson, S. Meidt, E. Murphy, P. Appleton, L. Armus, A. Bolatto, B. Brandl, D. Calzetti, K. Croxall, M. Galametz, K. D. Gordon, R. C. Kennicutt, J. Koda, O. Krause, E. Montiel, H.-W. Rix, H. Roussel, K. Sandstrom, M. Sauvage, E. Schinnerer, J. D. Smith, F. Walter, C. D. Wilson, and M. Wolfire. The Emission by

Dust and Stars of Nearby Galaxies in the Herschel KINGFISH Survey. *ApJ*, 738:89, September 2011. doi: 10.1088/0004-637X/738/1/89.

M. Sullivan, D. Le Borgne, C. J. Pritchet, A. Hodsman, J. D. Neill, D. A. Howell, R. G. Carlberg, P. Astier, E. Aubourg, D. Balam, S. Basa, A. Conley, S. Fabbro, D. Fouchez, J. Guy, I. Hook, R. Pain, N. Palanque-Delabrouille, K. Perrett, N. Regnault, J. Rich, R. Taillet, S. Baumont, J. Bronder, R. S. Ellis, M. Filiol, V. Lusset, S. Perlmutter, P. Ripoche, and C. Tao. Rates and Properties of Type Ia Supernovae as a Function of Mass and Star Formation in Their Host Galaxies. *ApJ*, 648:868–883, September 2006. doi: 10.1086/506137.

Y. Taniguchi. The Mahoroba Project — Deep Survey with an Optical Intermediate-Band Filter System on the Subaru Telescope. In N. Arimoto and W. J. Duschl, editors, *Studies of Galaxies in the Young Universe with New Generation Telescope*, pages 107–111, February 2004.

L. Wang. Dust around Type Ia Supernovae. *ApJ*, 635:L33–L36, December 2005. doi: 10.1086/499053.

X. Wang, L. Wang, R. Pain, X. Zhou, and Z. Li. Determination of the Hubble Constant, the Intrinsic Scatter of Luminosities of Type Ia Supernovae, and Evidence for Nonstandard Dust in Other Galaxies. *ApJ*, 645:488–505, July 2006. doi: 10.1086/504312.

X. Wang, W. Li, A. V. Filippenko, R. J. Foley, N. Smith, and L. Wang. The Detection of a Light Echo from the Type Ia Supernova 2006X in M100. *ApJ*, 677:1060–1068, April 2008a. doi: 10.1086/529070.

X. Wang, W. Li, A. V. Filippenko, K. Krisciunas, N. B. Suntzeff, J. Li, T. Zhang, J. Deng, R. J. Foley, M. Ganeshalingam, T. Li, Y. Lou, Y. Qiu, R. Shang, J. M. Silverman, S. Zhang, and Y. Zhang. Optical and Near-Infrared Observations of the Highly Reddened, Rapidly Expanding Type Ia Supernova SN 2006X in M100. *ApJ*, 675:626–643, March 2008b. doi: 10.1086/526413.

X. Wang, W. Li, A. V. Filippenko, R. J. Foley, R. P. Kirshner, M. Modjaz, J. Bloom, P. J. Brown, D. Carter, A. S. Friedman, A. Gal-Yam, M. Ganeshalingam, M. Hicken, K. Krisciunas, P. Milne, J. M. Silverman, N. B. Suntzeff, W. M. Wood-Vasey, S. B. Cenko, P. Challis, D. B. Fox, D. Kirkman, J. Z. Li, T. P. Li, M. A. Malkan, M. R. Moore, D. B. Reitzel, R. M. Rich, F. J. D. Serduke, R. C. Shang, T. N. Steele, B. J. Swift, C. Tao, D. S. Wong, and S. N. Zhang. The Golden Standard Type Ia Supernova 2005cf: Observations from the Ultraviolet to the Near-Infrared Wavebands. *ApJ*, 697: 380–408, May 2009. doi: 10.1088/0004-637X/697/1/380.

J. C. Weingartner and B. T. Draine. Dust Grain-Size Distributions and Extinction in the Milky Way, Large Magellanic Cloud, and Small Magellanic Cloud. *ApJ*, 548:296–309, February 2001. doi: 10.1086/318651.

L. A. Wells, M. M. Phillips, B. Suntzeff, S. R. Heathcote, M. Hamuy, M. Navarrete, M. Fernandez, W. G. Weller, R. A. Schommer, R. P. Kirshner, B. Leibundgut, S. P. Willner, R. P. Peletier, E. M. Schlegel, J. C. Wheeler, R. P. Harkness, D. J. Bell, J. M. Matthews, A. V. Filippenko, J. C. Shields, M. W. Richmond, D. Jewitt, J. Luu, H. D. Tran, P. N. Appleton, E. I. Robson, J. A. Tyson, P. Guhathakurta, J. A. Eder, H. E. Bond, M. Potter, S. Veilleux, A. C. Porter, R. M. Humphreys, K. A. Janes, T. B. Williams, E. Costa, M. T. Ruiz, J. T. Lee, J. H. Lutz, R. M. Rich, P. F. Winkler, and N. D. Tyson.

The Type IA supernova 1989B in NGC 3627 (M66). *AJ*, 108:2233–2250, December 1994. doi: 10.1086/117236.

M. Yamanaka, H. Naito, K. Kinugasa, N. Takanashi, M. Tanaka, K. S. Kawabata, S. Ozaki, S.-Y. Narusawa, and Sadakane Kozo. Early Spectral Evolution of the Rapidly Expanding Type Ia Supernova 2006X. *PASJ*, 61:713–, August 2009. doi: 10.1093/pasj/61.4.713.